ANALYSIS OF GEOTHERMAL PILE FOUNDATIONS UNDER COMBINED AXIAL AND MOMENT LOADING

BY

MICHAEL GRAY

A thesis submitted in partial fulfillment of
the requirements for the degree of

MASTER OF SCIENCE IN CIVIL ENGINEERING

WASHINGTON STATE UNIVERSITY
Department of Civil and Environmental Engineering

DECEMBER 2013

To the Faculty of Washington State University:

The members of the Committee appointed to examine the thesis of MICHAEL GRAY find it satisfactory and recommend that it be accepted

_____

Balasingam Muhunthan, Ph.D., Chair

_____

William Cofer, Ph.D.

_____

Haifang Wen, Ph.D.

ACKNOWLDEGEMENT

I would first like to thank my advisor and committee chair, Dr. Balasingam Muhunthan. You have repeatedly gone above and beyond the expectations of an advisor and professor in an effort to place my needs as a student first. Your advice and guidance with my thesis, as well as with your graduate courses, have readily prepared me for my career after studies.

Thank you to Dr. William Cofer for both your support and knowledge of finite elements, as well as granting me your confidence to serve on my committee. You have directed me with both my thesis research as well as the understanding of finite elements.

Thank you also to Dr. Haifang Wen for also serving on my committee. Your availability for answering questions and support is very much appreciated.

Special thanks to my girlfriend, Cristin Rocafort, who has stuck by my side during my graduate studies. Your patience and friendship is not neglected and I am grateful for everything you and your family have done for me.

Lastly, but not least, I would like to thank my parents, Stan and Rose Mary Gray, for their love, care and continued support throughout my entire life. They have instilled in me the integrity and attitude necessary to be not only a great engineer but also a great person.

ANALYSIS OF GEOTHERMAL PILE FOUNDATIONS UNDER COMBINED AXIAL AND MOMENT LOADING

ABSTRACT

by Michael Alex Gray, M.S.
Washington State University
December 2013

Chair: Balasingam Muhunthan

Geothermal pile foundations provide numerous advantages over conventional piles in terms of sustainability. Geothermal piles are similar to conventional reinforced concrete piles but with additional polyethylene tubing secured to the inside of the reinforcing cage. The additional tubing circulates a liquid which, when used with a heat pump system, can be used to heat and cool the structure the piles support. The heat transfer characteristics between geothermal piles and the surrounding soil have been investigated extensively, but very little research has been done examining the structural integrity or performance of the piles.

The structural performance of geothermal reinforced concrete piles was compared to conventional reinforced concrete piles using a cross sectional analysis program, Xtract, and the finite element program, Abaqus. Xtract was used to quantify and compare the differences in moment-curvature diagrams between cross sections with and without the tubing and Abaqus was used to develop a three dimensional model with similar cross sections to compare with Xtract.

Xtract results showed no differences between the various cross sections for curvature values up to 0.02 1/m. Curvature values in excess of 0.1 1/m showed marginal differences for the

estimated moment, except for the case of completely unconfined concrete. Curvature results from Abaqus results were within 30 to 40 percent of those predicted by Xtract for the finest mesh. Limitations due to convergence issues from the tensile behavior of the concrete prevented larger moments to be reached. The moment and curvature values of the model were only able to reach between 20 and 60 percent of the maximum moment predicted by Xtract.

The results from both Xtract and Abaqus showed that the structural performance of the pile is highly dependent upon the longitudinal reinforcement of the pile, rather than the confined concrete within the transverse reinforcement. Therefore, conventional and geothermal reinforced concrete piles perform similarly under static, axial, and moment loading conditions.

TABLE OF CONTENTS

LIST OF TABLES

LIST OF FIGURES

CHAPTER 1

INTRODUCTION

Background

Energy foundations utilize the necessary structural elements of a foundation and combine them with a geothermal energy transfer mechanism. Piles, diaphragm walls, basement slabs, tunnel anchors, and tunnel linings are just some of the foundation elements that have been combined with geothermal elements (Brandl, 2006). Geothermal piles, also referred to as heat absorber or energy piles, are a type of energy foundation which utilize subsurface geothermal energy to heat or cool the building which it supports. The first geothermal piles were built in Austria in the early 1980's, but have seen a large increase of installation taking place within the past decade (Brandl, 2006). There are many types of geothermal piles available. Driven steel and ductile cast iron, as well as pre-fabricated driven and bored cast-in-place reinforced concrete are the most common geothermal piles. The difference between typical piles and geothermal piles are the additional high-density polyethylene (HDPE) plastic pipes installed within the pile which circulates a heat transfer fluid. The fluid is then connected to a heat pump system installed within the building which is then used to heat or cool the building.

Implementation of geothermal piles, like any structure, has both advantages and disadvantages. Reduction of both fossil fuels and material contribute to a sustainable product. When designed properly, the recycling effect from drawing and depositing heat in the soil subsurface also contribute to the sustainable function of the foundation system. The initial cost is

larger than conventional systems because of additional design and material costs for both the foundation and the heat pump system. However, annual savings have been shown to have a payback period of less than 10 years for most systems (Brandl, 2006).

Use in areas where freeze-thaw cycles occur in soil should be avoided, as this can cause heave or settlement issues of the pile as well as possible damage to the heat transfer tubing. Additional care in construction should be taken when assembling the pile. In particular, the longitudinal and transverse reinforcement should be welded rather than tied in order to provide less flexure of the reinforcement cage, which limits the chances of damage to the heat transfer tubing. The heat transfer tubing should also be pressurized when pouring and forming the concrete of the pile (Brandl, 2006).

Geothermal piles include a more complex interaction between the soil and pile than conventional piles. A framework for understanding geothermal pile behavior is easily understood by considering or investigating the thermal loading, the mechanical loading, and the combined thermo-mechanical loading. The end conditions or restraint of the head and toe of the pile are shown to greatly affect the stresses and strains experienced within the pile.

While advances are being made in analysis of the geothermal response, their performance under dynamic loading is not yet understood. The pile-soil-structure interaction for geothermal foundations is not yet fully quantified, but they show promise in having the possibility to be implemented in many climates.

Objectives

The main objective of this study is to analyze the structural response under combined axial and moment loading of geothermal reinforced concrete piles and compare the results with that of conventional reinforced concrete piles. The effect of concrete removal, from the placement of additional vertical heat absorber tubing, on the performance of geothermal reinforced concrete piles will be analyzed using the cross sectional analysis program Xtract and the finite element software Abaqus.

The specific objectives of this research are to:

- Utilize the cross sectional analysis program Xtract to compare the structural performance of geothermal reinforced concrete piles with conventional reinforced concrete piles under combined axial and moment loading.
- Develop a 3D finite element model using Abaqus to investigate the effect of triaxial concrete behavior on the response.
- From results of both Xtract and Abaqus, evaluate and discuss the effect of heat exchanger tubing diameter, spiral and longitudinal reinforcement and soil type on pile performance.

Organization of Thesis

This thesis is organized into five chapters. Chapter 2 contains a literature review. It provides a background of the concepts, ideas, and procedures discussed later in the study. A summary of pertinent and related literature is also included in this section. Chapter 3 discusses

the Xtract program and how it was used to compare geothermal and typical reinforced concrete cross sections. Material inputs, pile layouts, and loading conditions will be discussed as a presentation of the results. Chapter 4 provides an introduction to Abaqus as well as how it was used to compare geothermal and typical reinforced concrete cross sections. Geometry, material models, boundary and loading conditions, and mesh sensitivity along with the results are also included. Lastly, Chapter 5 will provide a summary of the results and conclusions from the study. Suggestions as to how this research could be continued or improved upon for further study is also included.

CHAPTER 2

LITERATURE REVIEW

Introduction

The HDPE tubing is installed and secured to the steel reinforcing cage prior to placement of the geothermal reinforced concrete piles in the bore hole (Figure 2-1). Geothermal reinforced concrete piles can have the additional HDPE tubing installed vertically in the pile, which is most common, or it can follow the reinforcement cage in a spiral approach to tubing layout. The additional pipes are referred to as the heat exchanger or absorber tubing and when installed vertically it forms a U-shape. The heat transfer or carrier fluid is made up of either water, water and glycol, or a saline solution (Brandl, 2006). A mixture of glycol, anti-freeze agent, and water is the most commonly used fluid because of its resistance to expansion if temperatures of the liquid were to drop, which could lead to damage of the heat exchanger tubing. Both prefabricated driven piles and bored cast-in-place reinforced concrete piles make up the majority of installations for energy piles (Brandl, 2006).

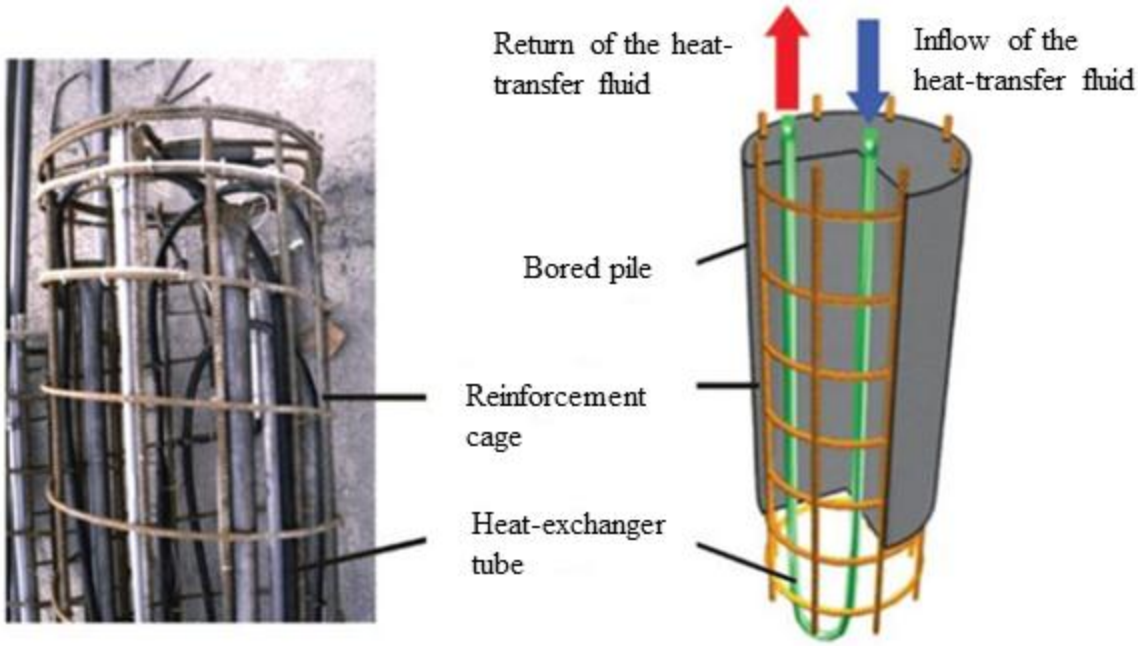

Figure 2-1: Energy pile layout (Laloui and Di Donna, 2011)

Energy piles make use of the great thermal transfer and storage properties of concrete to provide the medium through which thermal energy is transferred (Brandl, 2006). The piles act as the primary circuit of a ground source heat pump (GSHP) system, with the secondary circuit being the distribution or collection unit inside the building. Subsurface temperatures remain relatively constant between 10 to 24° Celsius at depths of greater than 6 m in most U.S. regions (Olgun et al., 2013). This energy source is utilized by energy piles and energy transfer is accomplished by pumping or circulating the carrier fluid which either injects or deposits thermal energy depending on the time of year. During the warmer summertime months, the ground temperature is much cooler than the outside temperature and the circulated liquid will transfer heat to the soil and groundwater surrounding the pile (Figure 2-2). This action cools the liquid which is then circulated back to the heat exchanger which will then be used to cool the

circulating air of the building and vice versa during the winter months. It should be noted that Figure 2-2 displays vertical boreholes that are placed directly in contact with the ground, however the seasonal performance is exactly similar to that of geothermal piles.

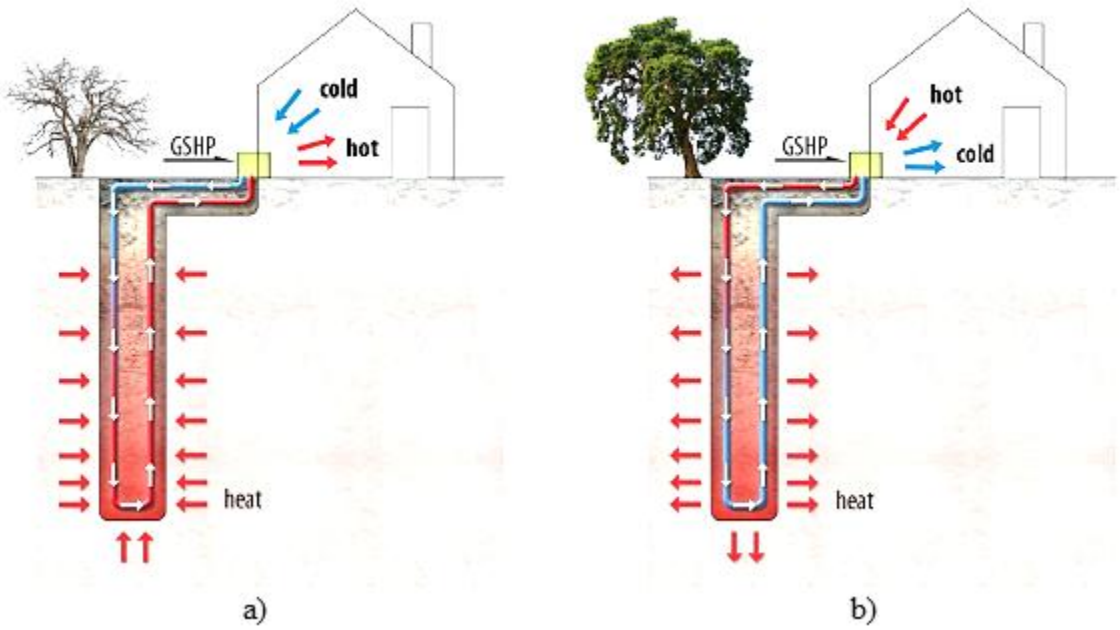

Figure 2-2: Seasonal operation diagram; a) winter, b) summer (Johnston et al., 2011)

The circulation and subsequent transfer of heat through the heat exchanger tubing applies additional thermal stresses and displacements along with those already experienced by the foundation from building loads (Laloui and Di Donna, 2011). Heat transfer in piles also affects the soil properties, which affect shaft resistance, tip resistance, or both (Brandl, 2006).

Currently there is no adopted standard for design of energy piles. Most design is based on past experience and tests results. This typically leads to overdesigned piles, with quite large employed factors of safety (Knellwolf et al., 2011). A more refined approach to energy pile

design can reduce construction costs as well as still provide the thermal and structural load capacities needed for the building.

The important distinction between energy piles and conventional piles is the additional transfer of thermal energy and the resultant increase in thermal stresses due to the heating/cooling cycles. Common piles expand and contract due to changes in temperature as well, but at a much smaller rate than that by energy piles.

The heat transfer tubing of geothermal reinforced concrete piles occupies area within the transverse reinforcement. The core of the pile, or the area within the hoop or spiral reinforcement, contains both concrete and longitudinal reinforcement. Concrete within the core is typically referred to as confined concrete and has increased compressive strength compared to unconfined concrete, or the concrete outside the transverse reinforcement. The reason for the increase in compressive strength is due to the limit of lateral deflection from the transverse reinforcement.

The reduction of confined concrete area by the heat transfer tubing and the effect on the structural performance of the pile has yet to be investigated by researchers. By researching the performance of both piles under static loading, a comparison can be made between both conventional and geothermal reinforced concrete piles. The results of static loading may also provide some knowledge about the dynamic or seismic response of geothermal piles.

The analytical response of geothermal piles is complex due to the interaction of soil, pile, and thermal behavior. However, following the methods of analysis proposed in pile design, equations to develop the response of geothermal piles under thermo-mechanical loading were proposed by Amatya et al. (2012) and Bourne-Webb et al. (2009 and 2012). The authors

proposed a framework for understanding the thermal and mechanical loading experienced by the pile dependent upon temperature change, end restraint, and material and thermal properties of the pile. Limited field trials have also been conducted that have given vital information on the geo-thermal response. The field observations have also been used in the development and validation of numerical models.

In addition to the static behavior of geothermal piles, the dynamic behavior has also yet to be examined. The dynamic behaviors of piles are important considerations that must be accounted for in design, especially in seismic regions. Various techniques and modeling approaches to the dynamic response of the piles are discussed.

Energy Pile Framework

Energy pile response to thermal and mechanical loading is complex. However, by first looking at each component individually it is easier to understand the combined effect of both mechanisms (Amatya et al., 2012; Bourne-Webb et al., 2012 and 2009).

Mechanical Loading Only

First consider a pile under axial loading only. The load is transferred to the surrounding soil at the toe, along the shaft, or a combination of both. The soil properties are largely responsible for how the load is distributed between the toe or shaft. The magnitude of the forces can be estimated once the soil stratigraphy is known. The mechanical load can be expressed as the following:

$$P_M = E_P A_P \varepsilon_M \tag{2-1}$$

where:

P_M = *mechanical load*

E_P = *Young's modulus of the pile*

A_P = *area of the pile*

ε_M = *mechanical strain of the pile*

The Young's modulus and area of the pile stay relatively constant with depth, but the mechanical strain and load can vary with depth and they are dependent upon soil and pile conditions.

A pile that is mostly supported at the toe is referred to as a point bearing pile and conversely, a friction pile if mostly supported along the shaft. Figure 2-3 displays the distribution of the mechanical strain (or axial load) and shaft resistance due to mechanical loading only for: a) friction, b) point bearing, and c) combined piles. Notice how the mechanical strain is largest at the surface, where the axial load is located, and decreases linearly for friction and the combined case along the length of the pile. The mechanical strain of the combined pile decreases at a smaller rate than the friction pile because the additional force at the toe of the pile decreases friction along the shaft. The shaft resistance diagram, q_s, is the derivative of the axial load diagram and is largest for the friction pile, which is to be expected. These are the extreme cases. In actuality, most piles are a combination of toe and shaft resistance but the axial diagram, and hence shaft resistance diagram, may not be linear and instead may be curved depending on the soil conditions and soil-pile interaction.

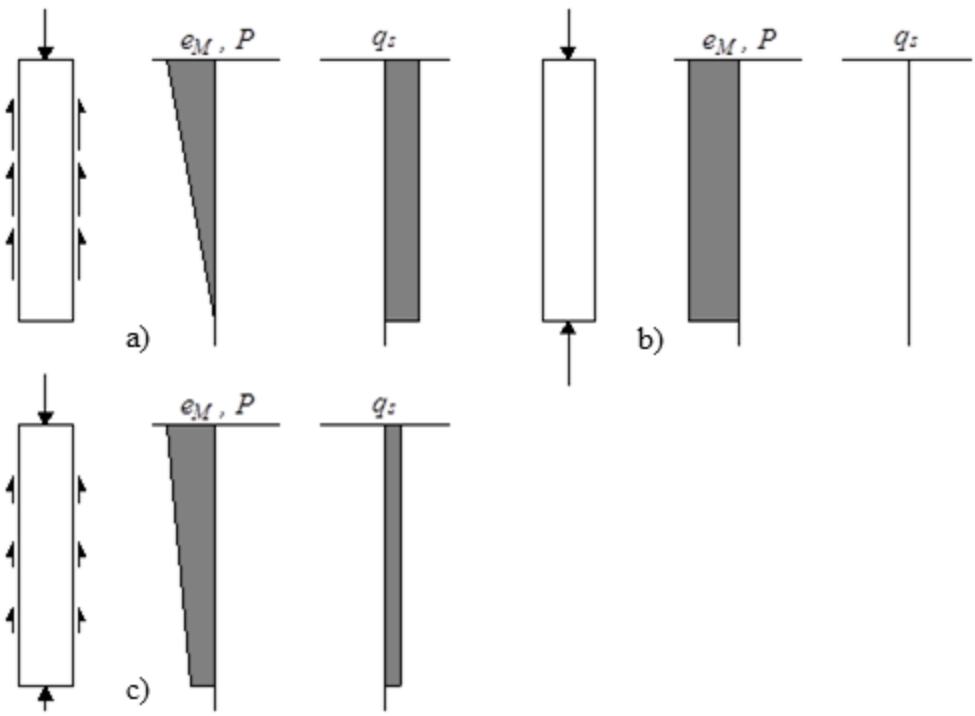

Figure 2-3: Mechanical loading pile diagram; a) friction, b) point bearing, c) combined (Bourne-Webb et al., 2012)

Thermal Loading Only

Consider a pile with no end restraints or axial loading. If the pile experiences a change in temperature, then a free thermal strain will develop according to the following (Amatya et al., 2012):

$$\varepsilon_{T-Free} = \alpha_P \Delta T \tag{2-2}$$

where:

α_p = *coefficient of thermal expansion for the pile and*

ΔT = *change in temperature experienced by the pile*

However, most piles are not free or without restraints. They may be restrained at the head, dependent upon the connection to the superstructure, the toe, dependent upon the bearing stratum the pile is placed on, or side restraint, dependent upon the shear stresses that are present between the pile and soil (Bourne-Webb et al., 2012). Along those lines, the actual or observed thermal strain in the pile will be less than the free thermal strain because no pile is perfectly free. The restrained strain is expressed as

$$\varepsilon_{T-Rstr} = \varepsilon_{T-Free} - \varepsilon_{T-Obs} \tag{2-3}$$

Stresses will manifest within the pile from the restrained thermal strains. All thermal strains are directly dependent upon the change in temperature of the pile. Again, if the pile is restrained and there is positive temperature change, such as during heating, the pile will expand, resulting in additional compression stresses and similarly a tension state during cooling. The resulting restrained thermal strains cause an induced thermal load expressed as

$$P_T = E_P A_P \varepsilon_{T-Rstr} = E_P A_P (\alpha_P \Delta T - \varepsilon_{T-Obs}) \tag{2-4}$$

The relationship between the free and restrained thermal strains and hence the induced axial loads is shown in Figure 2-4. The sign convention for the diagrams is shown with compression as positive and tension as negative.

As the pile expands or contracts from a temperature change, the surrounding soil also affects the induced axial load as well as the mobilization of a shaft resistance. The magnitude of the energy pile and soil response is again dependent upon both the temperature change and end restraint of the pile. Figure 2-5 provides the combined energy pile and soil response for both free and fixed end restraints during heating and cooling, as well as the mobilized shaft resistance. The soil response demonstrates the shaft resistance is opposite in direction for the top and bottom half

of the pile due to the contraction of the pile within the soil. The generated axial load from the soil response is largest at the midpoint of the pile and linearly decreases towards the endpoints. The overall axial load is highest for restrained endpoints because of the additional uniform axial load along the length of the pile. The mobilized shaft resistance is shown to increase in value with stiffer soils or larger temperature change for free piles and the opposite for restrained piles.

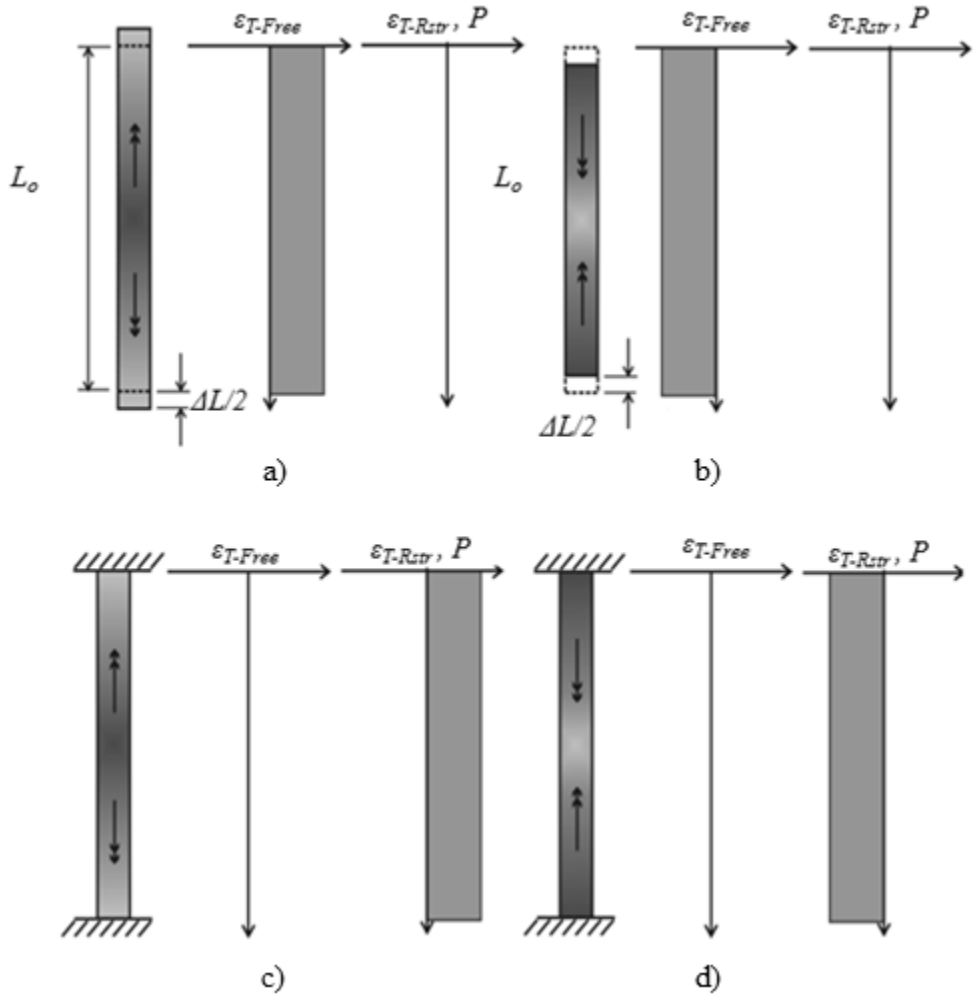

Figure 2-4: End restraint on geothermal pile response; a) free-heating, b) free-cooling, c) restrained-heating, d) restrained-cooling (Bourne-Webb et al., 2012)

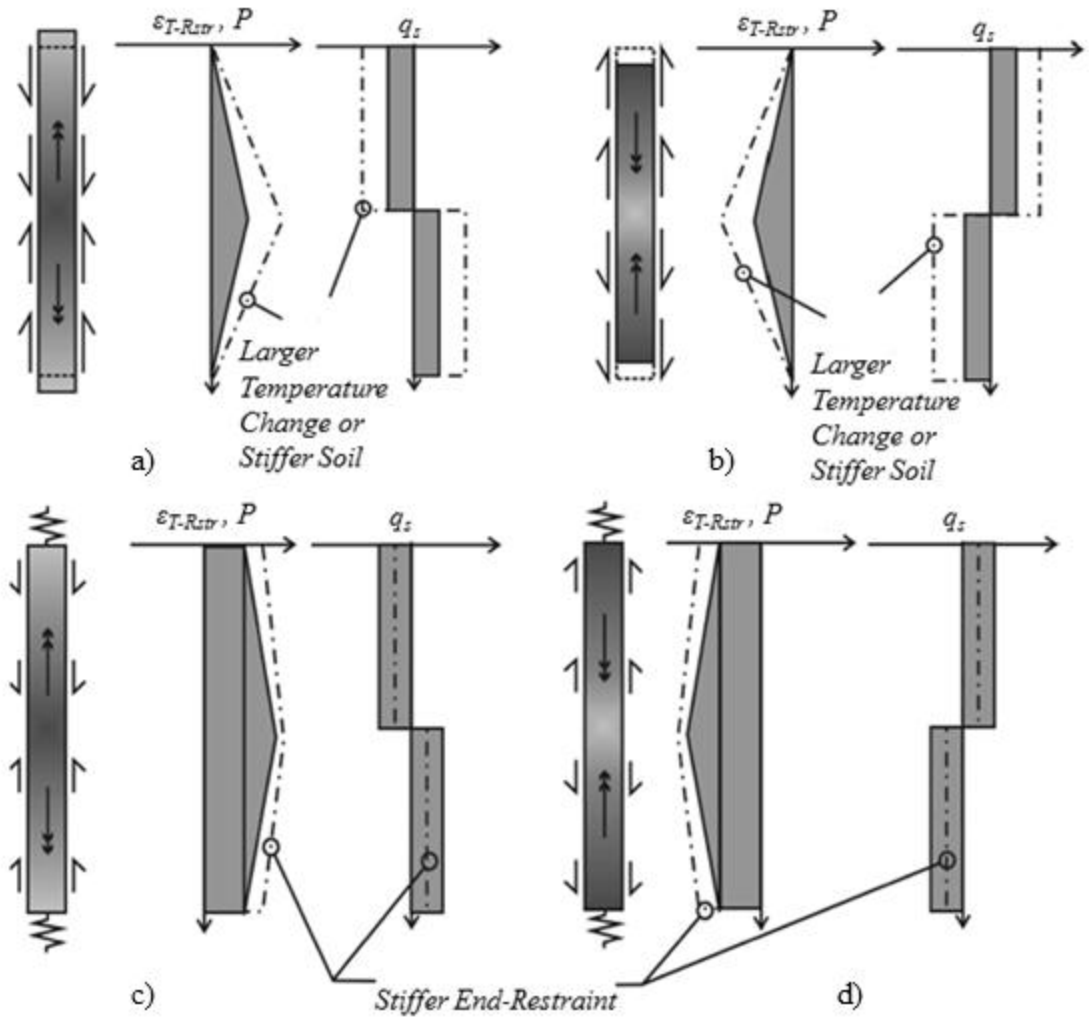

Figure 2-5: End restraint on geothermal pile & soil response; a) free and heated, b) free and cooled, c) restrained and heated, d) restrained and cooled (Bourne-Webb et al., 2012)

Combined Thermo-Mechanical Loading

Now consider the combined effect of both thermal and mechanical loading. If a temperature change is present as well as an axial load at the head of the pile, then the total mobilized strain can be estimated as

$$\varepsilon_{Total} = \varepsilon_M + \varepsilon_{T-Obs} \tag{2-5}$$

where:

ε_M = *mechanical strain due to the axial load*

$\varepsilon_{T\text{-}Obs}$ = *strain due to the thermal load*

The total load is the combination of both components superimposed. Therefore, the total load can be expressed as

$$P_{Total} = P_M + P_T \tag{2-6}$$

where P_M and P_T are as previously defined. The combined axial load and shaft resistance for the combined loading cases are presented in Figures 2-6 and 2-7. For Figure 2-6, the load is considered to be mobilised completely in the shaft, thereby neglecting end restraint conditions. However, they are considered in Figure 2-7. The dashed lines overlaid on the axial load and shaft resistance diagrams show the values for just the mechanical loading. Deviations from the dashed lines are from the thermal loading and all cases presented exhibit increases in either the axial load or shaft resistance.

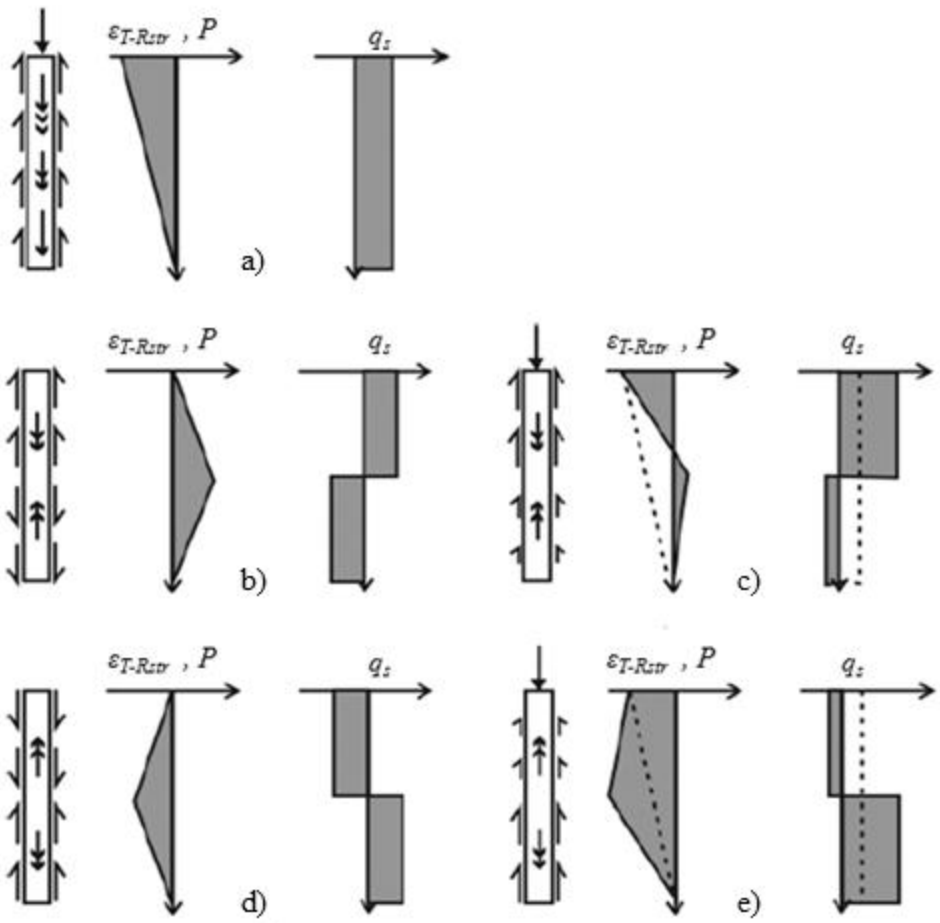

Figure 2-6: Energy pile response under thermo-mechanical loading; a) load only, b) cooling only, c) combined load and cooling, d) heating only, e) combined load and heating (Amatya et al., 2012)

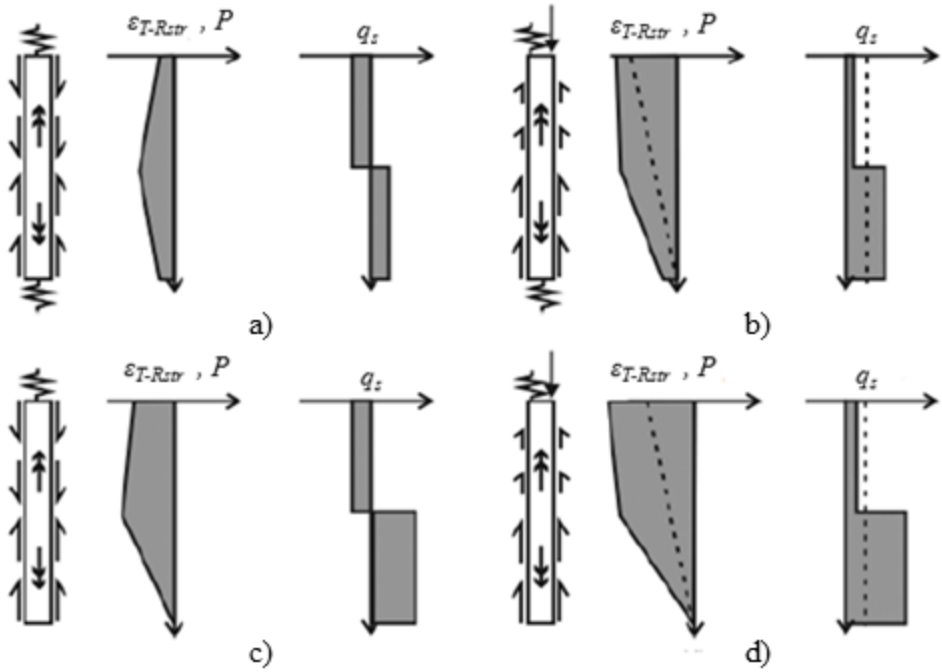

Figure 2-7: Energy pile response under thermo-mechanical loading with end restraint; a) partially restrained, b) combined load and heating, c) top restrained, d) combined load and heating (Amatya et al., 2012)

Energy piles have a unique and more complex framework than that of conventional piles because of the additional thermal loading. End restraint, temperature change, and soil strength properties all greatly affect the magnitude and distribution of the load throughout the pile, in particular the axial load and shear stress along the pile-soil interface.

Field Studies

Field results from London (United Kingdom), Lausanne (Switzerland), and Bad Schallerbach (Austria) are the three most discussed and well documented in the literature (Amatya et al., 2012; Bourne-Webb et al., 2012; Bourne-Webb et al., 2009; Brandl, 2006; Laloui et al., 2006). The following paragraphs are a summarized version. For a complete and thorough description of testing and results, one may refer to the references.

London, United Kingdom

Testing took place at Lambeth College and included two piles. The main test pile was 23 meters long and had an axial load of 1200kN applied as well as a thermal load. The heat sink pile was 30 meters long and only thermally loaded during testing. Both piles were placed in stiff, silty clay with the top 4 meters consisting of sand and gravel or granular fill.

Lausanne, Switzerland

Testing took place at Ecole Polytechnique Federale de Lausanne and included only one test pile. The pile was 25.8 meters long and part of a four story building that was monitored during construction and included both mechanical and thermal loading during testing. Thermal tests were done at the completion of each of the four stories and consisted of a heat and recovery period lasting 28 days. In total, eight tests took place during construction of the building. The pile was placed in various layers of clay and terminated in a moderate to weak sandstone.

Bad Schallerbach, Austria

Testing took place at a rehabilitation center in Bad Schallerbach. It was a relatively short energy pile, 9 meters long, and was placed in a two layered sand and clayey silt. Testing took place at various times of the year over several years of operation during pre and post construction.

Field Study Results

The induced axial stress generated within the pile from thermal loading was within 50 to 100 percent of the estimated completely restrained values. The mobilized shaft resistance during thermal loading was also seen to increase as expected, and larger changes were seen in stiffer soils.

The three summarized field trials are helpful in quantifying energy pile behavior, but each reported test has limitations in reported values. The London piles used larger than typical temperature cycles and had a limited testing time frame. The Lausanne pile was placed within a foundation system of conventional piles which most likely led to much larger stress during thermal loading at the head of the pile. The Lausanne pile was also only exposed to heating cycles and the Bad Schallerbach pile only reported a few values each year.

The fully restrained values would provide the largest factor of safety during design and should be used until further development and understanding of the effect of changes in the magnitude of different end restraints are understood. The prediction of shaft resistance is quite

complicated and difficult to predict, especially in layered soils. However, the thermal cycles of an energy pile most likely will not cause serious damage or failure if concrete stresses are accounted for, settlements are limited, and factors of safety used for end bearing and skin friction are maintained.

Numerical Methods

A few numerical and finite element methods have recently been developed to model energy piles. This technique can better predict the performance of the complex system that energy piles are a part of and there are currently a few published models that have been used to predict or model energy pile behavior.

Laloui et al. (2006) were among the first to use finite elements to model energy piles and compare the results with those obtained from the field trial results at Lausanne. The single energy pile was installed vertically within horizontally layered soil and a horizontally present groundwater table. The cross section dimensions and boundary conditions are presented in Figure 2-8. The mesh was refined at interfaces and quadratic elements were used for displacements. Bi-linear elements were used for pore water pressures and temperatures.

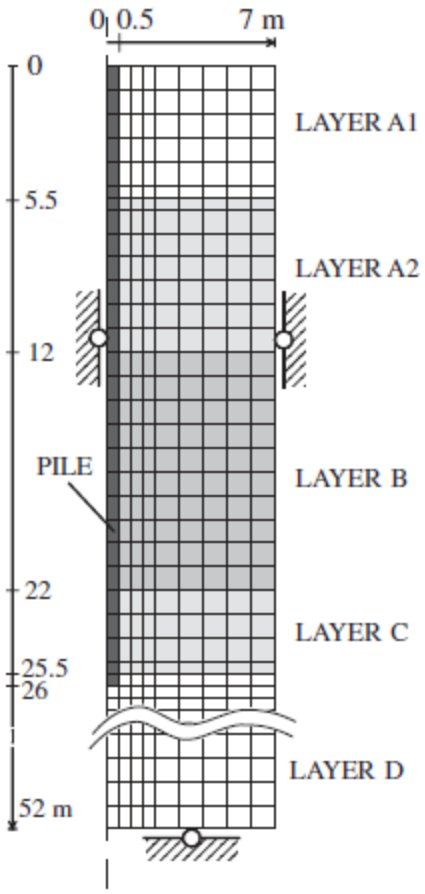

Figure 2-8: Finite element mesh and boundary conditions for Laloui et al., 2006

The pile-soil contact was considered rough, so no relative movement was allowed between the two surfaces. The pile was considered impervious and modeled as a thermo-elastic material. The pile properties were determined from a combination of both laboratory and ultrasonic transmission tests. The soil properties were determined through tri-axial tests and modeled using the Drucker-Prager thermo-elastoplastic model. All soil layers except layer D were considered drained. Therefore, from the boundary conditions, drainage may occur at the top and to the right of the model. The initial stress in the soil layers and pile was computed assuming

a coefficient of earth pressure at rest. Thermal boundary conditions consisted of a constant temperature along the top surface and heat flux was considered zero along the axis of symmetry. Therefore, heat flow could occur at both the right and bottom sides of the mesh. For evaluation, the temperature along the top surface and in the pile were applied that followed that of the values determined from a 12 day heating ($\Delta T = 21°C$) and 16 day cooling ($\Delta T = 3°C$) test period.

Two setups were considered; the first was equivalent to thermal loading only and the second was both mechanical and thermal loading. The models were evaluated using both a thermo-mechanical and thermo-hydro-mechanical model. The results showed that additional thermal loading produced considerably larger axial loads and were especially prevalent at the toe of the pile. The first model showed relatively no stress at the toe of the pile, however it only considered thermal loading and dead weight. The pile was shown to settle during static loading and elevate during thermal loading because friction resistance was shown to not be affected by temperature. However, relaxation of side friction was noticeable during heating cycles. The thermo-hydro-mechanical model produced similar results to the experimental values. The model also showed that if temperature change reaches soil particles, then the induced strain is restricted and does not affect the pore water pressure or effective stresses.

Knellwolf et al. (2011) followed up on the work by Laloui et al. (2006) and proposed a new model that discretized an energy pile into small segments. The segments were then analyzed and variations in soil properties or soil layer changes as well as changes in temperature were applied to the discrete elements. An iterative approach was used to solve for the strains and stresses during thermo-mechanical loading. The model did not, however, consider changes in the soil properties with temperature change and it has been shown that some thermal induced strains

are never fully recovered during temperature cycles in soil. The temperature cycles do affect the soil-pile interface because of the thermo-elastic response of the pile and the thermo-elasto-plastic response of the soil. This approach has shown promise and has since been commercialized into a computer software program, Thermo-Pile, utilizing the same model as published in the paper. It allows the user to input soil and pile properties along with estimated temperature changes to evaluate the response. The software also can account for floating, semi-floating and end-bearing piles, which are helpful in determining end restraint of the pile and quantifying additional effects of thermal loading.

Ouyang et al. (2011) utilized a numerical model to predict energy pile settlement and compared his model to the London field trial results. The model uses a hybrid load transfer approach that analyzes the pile-soil interaction with thermal loading and the pile-soil-pile interaction with an elastic continuum approach. The soil was modeled using a linear elastic/perfectly plastic soil. Thermal loading was shown to modify the shaft friction along the length of the pile and also shows the variation of loading and unloading transfer diagrams. The latter is important in determining the long term effects of thermal loading of energy piles. The results of the model showed similar comparisons, but also indicated that further understanding of the soil-pile interactions during thermal loading will lead to a more refined prediction model. Changes such as load-displacement relationships and radial expansion/contraction of pile could increase the models efficiency. The proposed model may be used to predict energy pile group performance, but no field trial results of energy pile groups are available.

Dynamic Pile Framework

Dynamic events such as earthquakes are typically of short duration. Therefore, consideration of the thermal-mechanical interaction during such an event is unwarranted. Instead, initial stress conditions brought on by thermal stresses and strains throughout the pile can be applied to study the soil-pile-structure interaction (SPSI).

SPSI analyses are done by considering the structure and soils together or by using the principle of superposition. The principle of superposition considers both kinematic and inertial interactions. This approached is best used for linear systems, but provides valid approximations for nonlinear systems (Balendra, 2005).

Several methods are used to study SPSI problems. The finite element method, boundary element methods, and beam on Winkler foundation models, semi empirical and semi analytical methods, and analytical solutions have all been used to study SPSI problems (Balendra, 2005). The Master's Thesis by Greenwood (2008) provided a starting point for modeling a pre-stressed concrete bridge column which was investigated using the software programs Xtract, SAP, and Abaqus. Figure 2-9 provides a visual of in situ modeling of a pre-stressed concrete column using Abaqus. This research will follow the work done by Greenwood for geothermal piles.

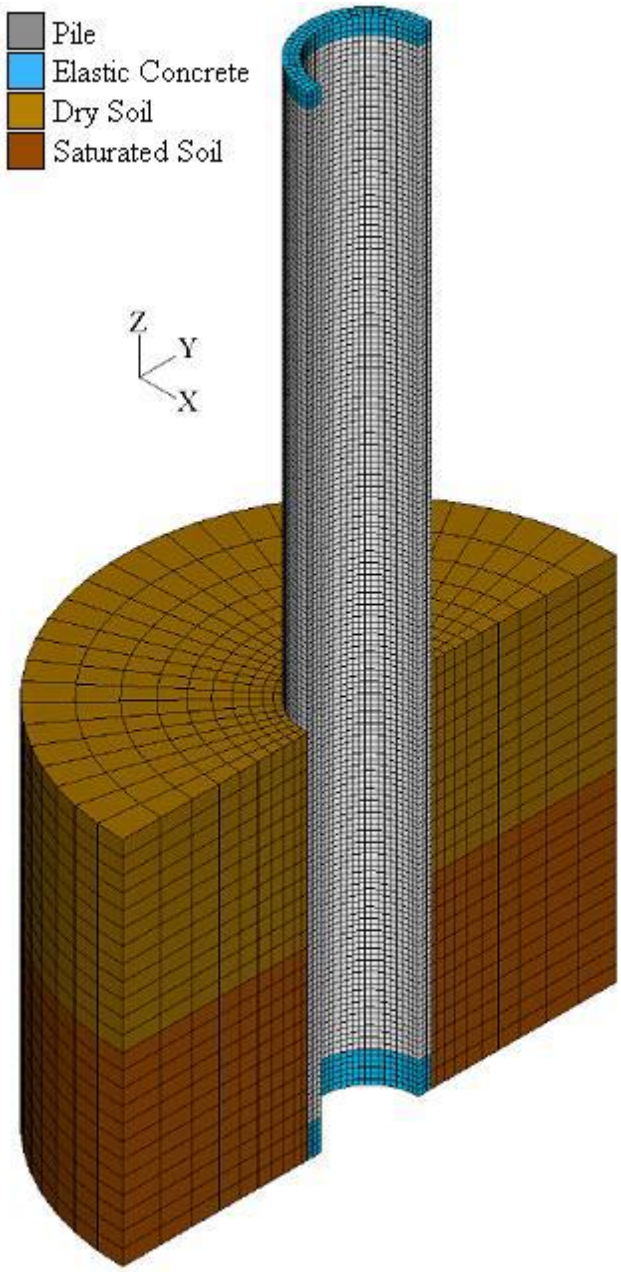

Figure 2-9: In-situ pre-stressed pile model in Abaqus (Greenwood, 2008)

Summary

Most energy piles constructed are designed based on past experience and empirical values with no complete step by step design process available. The thermal transfer between the soil-pile interface is understood fairly well with numerous past experiences on which to base designs for. The energy pile, specifically, the pile-soil interaction is little understood because of the very few published reports of energy pile field data available. This leads to most energy piles being overdesigned, resulting in larger construction costs. A comprehensive design procedure would lead to more economical or optimized designs of energy piles.

Energy piles experience a complex pile-soil interaction during heating/cooling cycles. While the pile experiences a thermo-elastic response, the soil experiences a thermo-elasto-plastic response (Knellwolf et al., 2011). Shear stress mobilizes at the soil-pile interface as well as additional stresses brought on by varying degrees of end restraint of the pile. Some published models are available that help to capture and predict energy pile response in certain soil/pile conditions, but do not yet provide a complete model that can be adjusted to correctly or accurately model most soil/energy pile setups.

CHAPTER 3

ANALYSIS OF GEOTHERMAL PILE PERFORMANCE USING XTRACT

Pile Description

A typical cross section of a geothermal pile and a conventional reinforced pile are shown in Figure 3-1. As mentioned in Chapter 2, the heat transfer tubing is secured to the inside of the reinforcement cage in either a vertical or spiral arrangement, the former of which is more common. The removal of confined core concrete for purposes of heat transfer may compromise the stability of the piles. In order to study such effects, if any, analyses of various configurations were conducted. The first series of analyses were conducted using Xtract and the second series were conducted using Abaqus by comparing piles with and without the removal of concrete from heat transfer tubing placement.

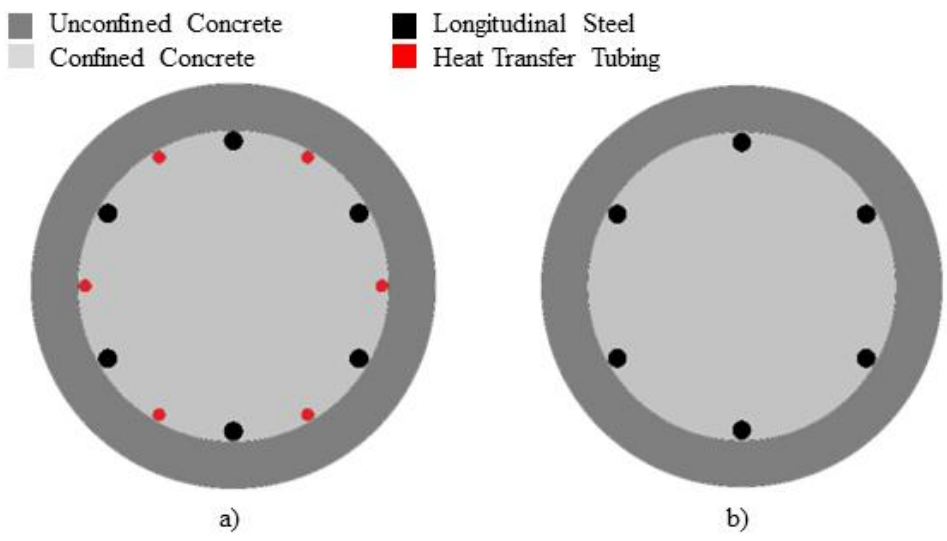

Figure 3-1: Reinforced concrete pile cross sections; a) geothermal, b) conventional

Introduction

Xtract is a software tool used to analyze two dimensional cross sections subjected to axial and/or moment loading. The cross sections can be defined from the available built-in templates, a user defined section or an imported section file. Nonlinear material models are available and once defined, can be applied to any of the available geometric entities defined within the cross section. Once the geometry and material models are defined, the cross section can be discretized into smaller elements.

There are three analysis types available in Xtract; moment-curvature, axial-force moment interaction, and moment-moment interaction also called capacity orbit (TRC/Imbsen Software, 2013). For this research project, the moment-curvature was analyzed for various cross sections. There are three available ways for solving the moment-curvature analysis; two force controlled methods and one displacement controlled method that all use an iterative nonlinear solver. The two force controlled methods include the iteration at a minimum unbalanced displacement norm and iteration at constant arc length method. Both methods increment the moments and forces to then find the corresponding curvatures and strains in the cross section. The displacement controlled method or the bisection method increments the curvatures or strains throughout the cross section. A linear strain distribution is assumed throughout the cross section for the displacement controlled method of the bisection method. The curvature is then incremented and the corresponding strains are determined in each element. From the defined material models the stresses in each element can be determined. The iterative solver then locates the neutral axis from the resultant forces calculated from the determined stresses. Lastly, once the resultant forces and the neutral axis are determined, the moment within the cross section can be determined.

The bisection method almost always converges and is best used for symmetric cross sections. If an asymmetric cross section is examined using the bisection method, it should be noted that although the curvature will be parallel to the direction of loading, the resultant moments will not. Therefore, the force controlled method should be employed when analyzing an asymmetric section.

Model Formulation

A pile diameter of 0.6 m was examined for all cross sections. Each pile cross section consisted of a circular cross section with spiral reinforcement. The spiral reinforcement consisted of 14mm bars spaced at 70mm and with a concrete cover of 70mm. The longitudinal reinforcement consisted of six 30mm bars evenly spaced. This resulted in a longitudinal reinforcement ratio of 1.5 percent.

Three material models were defined for the model: unconfined concrete for the concrete surrounding the spiral reinforcement, confined concrete for the concrete contained within the spiral reinforcement, and a parabolic strain hardening model for both the longitudinal and spiral steel reinforcement.

The unconfined concrete model is based on typical values as detailed by ACI specification. The input values used to define the unconfined concrete model are included in Table 3-1. The elastic modulus of the concrete was estimated by:

$$E_c = 4733 * \sqrt{f'_{uc}} \tag{3-1}$$

where:

f'_{uc} = 28-day unconfined compressive strength (MPa)

Equation 3-1 is a metric equivalent proposed by the ACI. The compressive strength was assumed to be 32.00 MPa and the elastic modulus was found to be 26.77 GPa. The tensile strength was defined by:

$$f'_{ts} = 0.62 * \sqrt{f'_{uc}} \tag{3-2}$$

based on ACI standards, with f'_c as previously defined. The tensile strength was found to be 3.50 MPa. The yield crushing strain, and spalling strain were left as the default values. The failure strain was set to 1, which will allow the program to continue to operate even after concrete spalling or crushing is reached in the unconfined concrete elements.

The confined concrete model was based on the work by Mander et al. (1988). The confined concrete strength is expressed as:

$$f'_{cc} = f'_{uc}\left[2.254 * \sqrt{1 + \frac{7.94 * f_{cp}}{f'_{uc}}} - \frac{2 * f_{cp}}{f'_{uc}} - 1.254\right] \tag{3-3}$$

where:

f_{cp} = confining pressure due to transverse steel.

f'_{uc} is as previously defined and it is important to note that Eq. (3-3) is only applicable for units of psi. The confining pressure due to transverse steel is defined as:

$$f_{cp} = 0.5 * k_e * \rho_s * f_{yh} \tag{3-4}$$

where:

k_e = confinement effectiveness coefficient

ρ_s = transverse reinforcing ratio

f_{yh} = yield strength of transverse reinforcement

The confinement effectiveness coefficient is defined as:

$$k_e = A_e * A_{cc} \tag{3-5}$$

where:

A_e = *effective area*

A_{cc} = *confined concrete area*

The confinement properties of the concrete were determined directly from the defined template values such as reinforcement size and spacing of the pile cross section. This made altering the cross section for the subtraction of concrete materials to represent the HDPE heat transfer tubing quite simple. The elastic modulus, compressive strength and tensile strength are assumed to be the same as that for the unconfined concrete model. The model parameters used here are shown in Table 3-1.

A bilinear steel with strain hardening model was used to describe the longitudinal steel based on A615 Grade 60 steel. Nominal properties for the steel were used and are included in Table 3-2.

Table 3-1: Xtract concrete properties

Elastic Modulus	26770 MPa
Compressive Strength	32.00 MPa
Post Crushing Strength	0 MPa
Tensile Strength	3.50 MPa
Yield Strain	1.40E-03
Crushing Strain	4.00E-03
Spalling Strain	6.00E-03
Failure Strain	1.00E+00
Compressive Strength (Confined)	52.15 MPa
Yield Strain (Confined)	5.808E-03
Crushing Strain (Confined)	20.00E-03

Table 3-2: Xtract steel properties

Elastic Modulus	199.9 GPa
Yield Stress	413.7 MPa
Fracture Stress	620.5 MPa
Strain at Strain Hardening	8.00E-03
Failure Strain	90.00E-03

Five cross sections were analyzed. Cross section 1 was the control with confined concrete defined within the spiral reinforcement and no holes (Fig. 3-2, a). Cross section 2 consisted of six 40 mm diameter holes spaced evenly between the longitudinal reinforcement and confined concrete in the core (Fig. 3-2, b). Cross sections 3 and 4 were the same as section 2, but with a 20 mm and 40 mm radial layer, respectively, of unconfined concrete surrounding the holes (Fig. 3-2, c and d). Cross section 5 consisted of the same 40 mm diameter holes but with the core concrete considered unconfined (Fig. 3-2, e). Heat exchanger tubing typically ranges from 20

mm to 40 mm in diameter, the latter of which was chosen because it should affect the pile performance more greatly.

Moment-curvature analysis for each pile cross section was performed using two steps. The first step was the application of an axial load to the cross section to simulate the vertical loading applied to the pile. The axial pressure or force was determined using:

$$F_a \leq 0.33f'_{uc} \tag{3-6}$$

as specified by the ACI code (Coduto, 2011). The maximum recommend axial force for a 0.6 m diameter pile and 32 MPa unconfined compressive strength would be around 1.2 MN. A value of 1 MN satisfies this requirement as was used as the axial force applied to each cross section. The next step involved incrementing the moment about either the x or y axis. This was performed because each cross section is not symmetric about both axes, and therefore, results for the moment-curvature of the piles will vary about each axis.

The moment-curvature relationship for each cross section about an equivalent axis was then plotted. Differences between the cross sections could then be compared and analyzed and the differences between the cross sections distinguished.

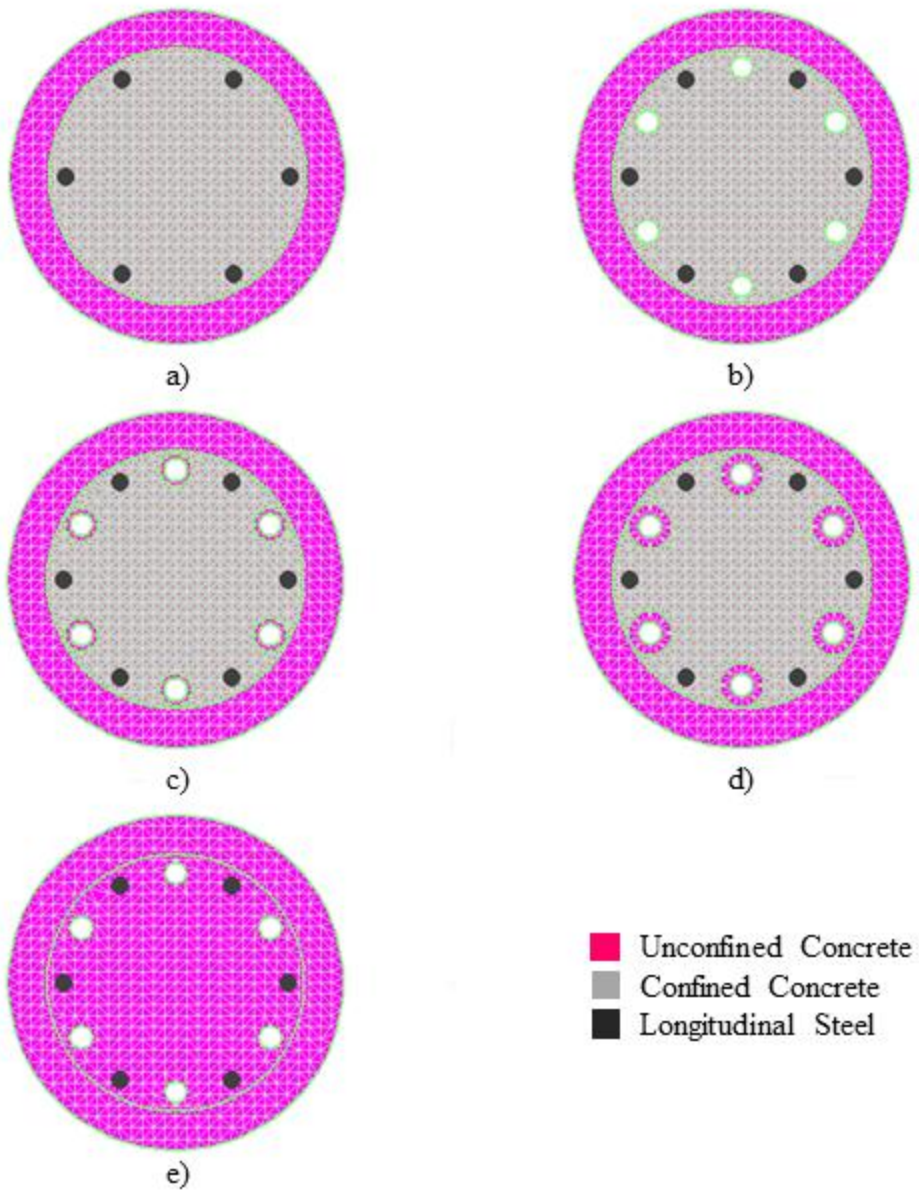

Figure 3-2: Defined cross sections

A mesh sensitivity analysis could not be carried out due in part to limitations of the software. As mesh size was decreased from an original value suggested by the software, a limit was reached that would cause an error in the program to occur. The limit seemed to be somewhat

related to the diameter of the pile being analyzed. The mesh size was therefore set at the smallest limit, to the nearest 5mm, without causing errors for each diameter of pile. The global element mesh size was set at 20mm for all cross sections.

Results

Results from the Xtract moment-curvature analysis about the x and y axis are included in Figures 3-3 and 3-4, respectively. No difference between the conventional reinforced concrete pile and those with modifications is observed for curvature values up to 0.02 1/m. At larger curvature values differences between the cross sections become apparent. Section 1 results provide the highest capacity which is to be expected because it is modeled as the conventional reinforced concrete pile, with no reduction in concrete due to heat absorber tubing. Tables 3-3 and 3-4 provide the percent difference in moment compared to that of section 1 for sections 2-5 about both the x and y axis, respectively, at various curvature values. The addition of holes (section 2) lowers the capacity only slightly by between 1 and 2 percent about both the x and y axis. The inclusion of unconfined concrete surrounding the holes (section 3 and 4) lowers the capacity further and the larger radius of unconfined concrete marginally more. Section 3 saw a reduction by about 3 or 4 percent at higher curvature values and section 4 by about 5 and 7 percent. For section 5, which considers holes as well as entirely unconfined concrete, moment capacity was greatly reduced, by between 50 and 60 percent at 0.1 1/m curvature values.

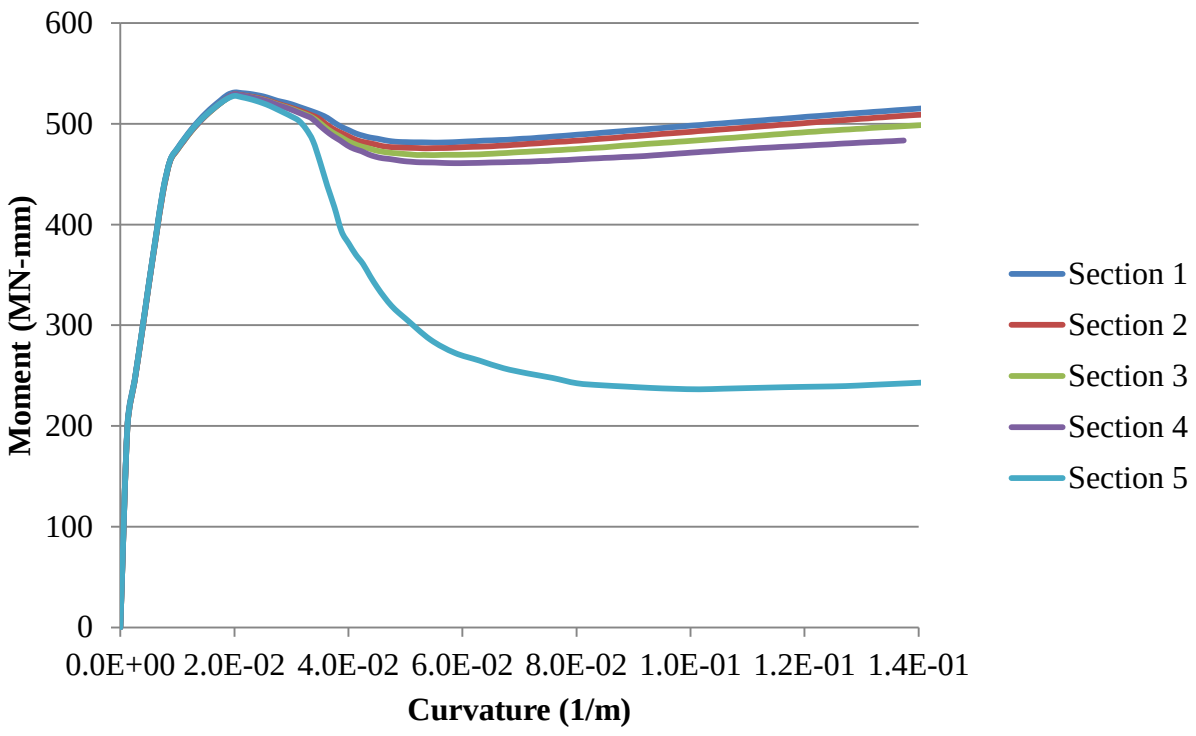

Figure 3-3: Moment-curvature results about the x axis

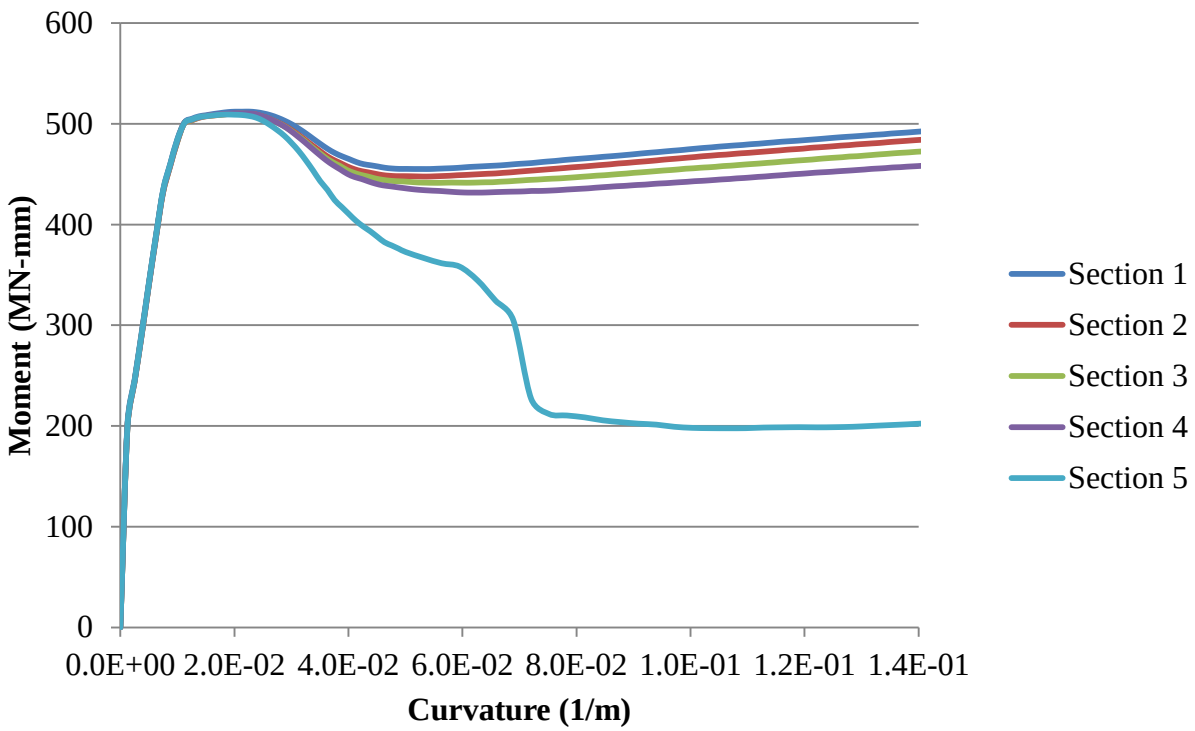

Figure 3-4: Moment-curvature results about the y axis

Table 3-3: Moment reduction values about x-axis

Curvature (1/m)	% Difference in Moment			
	Section 2	Section 3	Section 4	Section 5
0.020	0.38%	0.43%	0.38%	0.64%
0.040	1.05%	2.07%	3.04%	22.77%
0.060	1.12%	2.66%	4.38%	45.03%
0.080	1.27%	2.94%	4.99%	50.45%
0.100	1.28%	3.07%	5.42%	52.57%

Table 3-4: Moment reduction values about y-axis

Curvature (1/m)	% Difference in Moment			
	Section 2	Section 3	Section 4	Section 5
0.02	0.41%	0.43%	0.29%	0.59%
0.04	1.51%	2.32%	3.14%	11.70%
0.06	1.60%	3.29%	5.39%	21.53%
0.08	1.81%	3.96%	6.47%	54.97%
0.1	1.75%	4.10%	6.80%	58.32%

The differences between moment-curvature about the x and y axis are shown in Figure 3-5. At curvatures greater than 0.02 1/m the maximum moment about the x axis is larger than that for the y axis. Observation of the defined cross sections (Figure 3-2), shows that there is more steel present about the y axis through the center of the cross section than the x axis. This should have resulted in a higher moment-capacity about the y axis. However, due to the increment in applied moment, the neutral axis shifts horizontally till it is parallel with the two longitudinal reinforcement bars. As a result, the neutral axis relocates to nearly directly on top of these steel bars. Thus, they will not provide additional capacity resulting in observed reduction of moment-curvature capacity about the y axis (Figure 3-5).

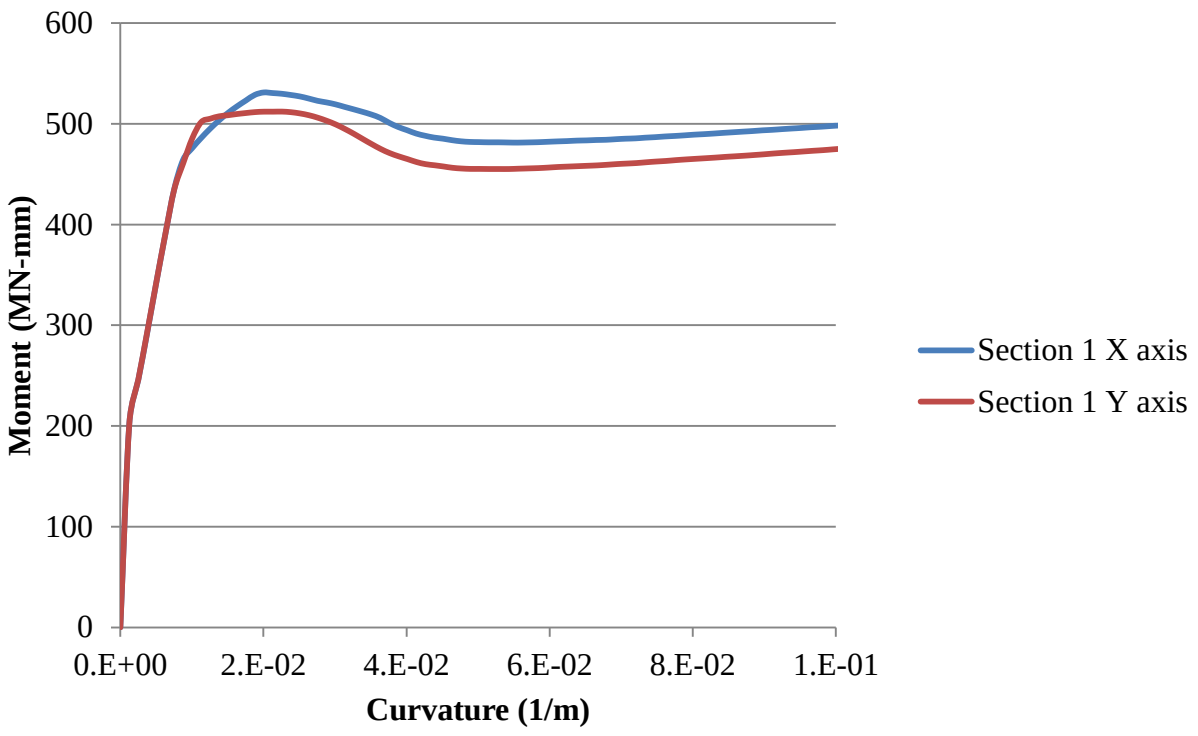

Figure 3-5: Moment-curvature comparison about axes

The progression of stress changes with application of moment at various locations on the moment-curvature diagram is shown in Figure 3-6 with the stress conditions in the cross sections about the x axis associated with locations a through g, shown in Figure 3-7. It is seen that, due to the combination of applied axial force and increment in applied moments, the top half is in tension and the bottom half is in compression throughout the analysis. At point *a* the cross section is evenly compressed due to the initial applied axial force. At point *b* the tensile strain in the longitudinal steel located the furthest away from the neutral axis has reached that required to cause initial yield of the steel. At point *c* both the longitudinal steel located at both the center and furthest from the neutral axis reached the tensile strain required to cause yield stress in the steel. At point *d* the tensile strain has increased to large enough to cause strain hardening in the

longitudinal steel furthest away from the neutral axis. At point *e* the compressive strain has reached the amount to cause spalling of the unconfined concrete and initial yield of the longitudinal steel at the lower part of the cross section. At point *f* the tensile strain for the centrally located longitudinal bars has reached that required to cause strain hardening of the steel. Lastly, at point *g* the compressive strain in the lower longitudinal bars has reached that required to cause strain hardening of the steel.

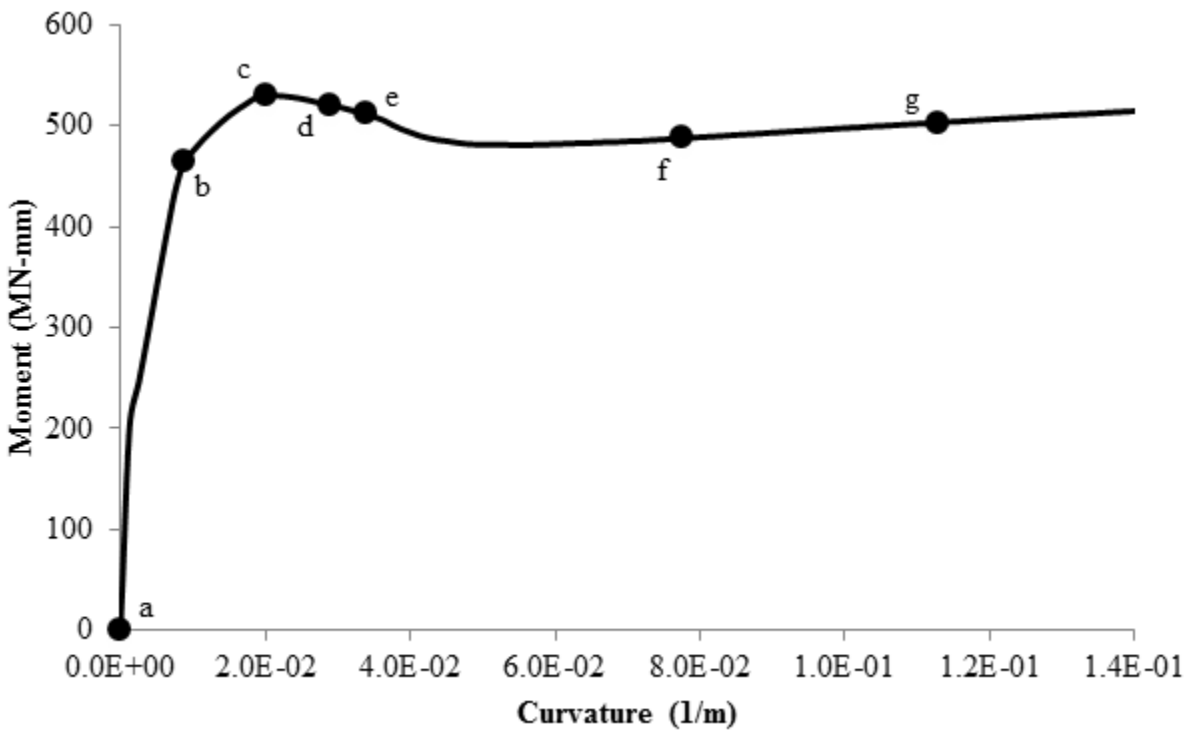

Figure 3-6: Locations of changes in stress conditions on the moment-curvature diagram

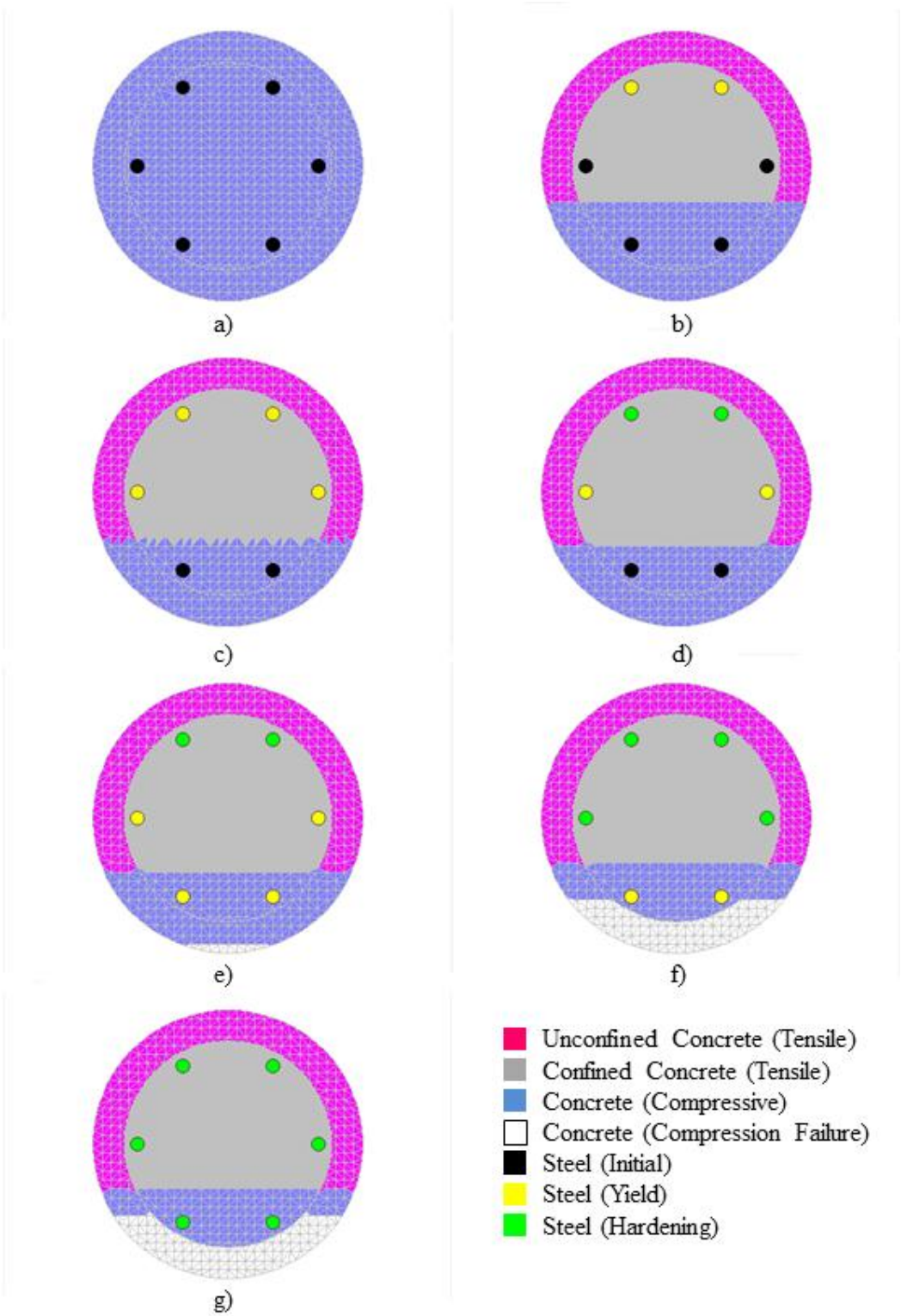

Figure 3-7: Pile cross section with changes in stress on moment-curvature diagram

CHAPTER 4

FINITE ELEMENT ANALYSIS OF GEOTHERMAL PILE PERFORMANCE

Introduction

The performance of a geothermal pile under combined axial load and moment is studied in this chapter using the finite element method (FEM). This technique is utilized by numerous engineering disciplines because it can provide numerical approximations to very complex systems. The FEM is carried out by discretizing a body into smaller parts called elements. Each element has a system of equations that are continuous across the entire element and described by the element nodes. Elements are connected to other elements by nodes and are where evaluation of the system takes place. Applied loadings to the element result in displacements which are then transformed back to a global coordinate system where the solutions can be viewed.

There are numerous FE software programs available, and the program Abaqus is used in the analyses reported here. Abaqus is a general-purpose software program that can perform both linear and nonlinear analyses. Since the original development in the late 1970's by Hibbitt, Karlsson & Sorenson, Inc., the program has undergone several advances (Liu et al., 2003). Abaqus/CAE version 6.11 is used here.

Abaqus/CAE is divided into two procedures, pre-processing and post-processing. Pre-processing defines all of the needed information to describe the system and the items that will be computed. This procedure contains distinct modules, with each module contributing to the modeling process. Once each module is completed, the model continues to progress and

advances and once the input file is complete it is submitted for analysis. Post-processing occurs after the analysis is complete. This procedure allows the results, as defined in the pre-processing, to be viewed, expressed, or examined in various ways.

There are no specified units in the Abaqus/CAE program leaving it up to the analyst to input and maintain consistent units throughout the modeling process. S.I. units (MPa-m) were chosen and used throughout the modeling process.

Model Geometry

Two different pile cross sections were analyzed. A conventional reinforced concrete pile that included no holes throughout the cross section and a geothermal reinforced concrete pile that included six 40 mm holes spaced evenly between the longitudinal steel throughout the length of the pile (Figure 4-1). The diameters of reinforced concrete piles have varied between 0.5 m to 1.2 m and their lengths between 10 and 30 m. The diameter of the pile considered here was defined to be 0.6 m. Since our focus here is on comparing moment-curvature results with that of Xtract (analyses reported in Chapter 3), consideration is given only to the top 1 m length of the pile. This length was chosen to be larger than one and a half times the diameter of the pile to allow for dissipation of loading conditions on the free end of the pile. To account for dissipation of discontinuities at end conditions, 0.6 m from the free end of the pile was defined using a concrete elastic material model. The remaining length of the pile was defined using the concrete damaged plasticity material model.

The schematic diagrams of the piles with loading are shown in Figure 4-2. The piles were also analyzed with and without a linearly increasing confining pressure to simulate lateral pressures applied to the pile from both a clayey and sandy soil.

The hoop reinforcement was comprised of 14 mm bars spaced 70 mm from the secured end of the pile. The longitudinal steel reinforcement consisted of six 30 mm bars evenly spaced throughout the cross section. The longitudinal and heat transfer tubing was placed just inside the hoop reinforcement which was located 70 mm from the exterior of the concrete. Transverse reinforcement in reinforced concrete piles is typically achieved by either spiral or hoops, the former of which is more common. To simplify the model, the transverse reinforcement was considered as hoops. The reinforcement layout is shown in Figure 4-3 and the defined reinforcement area is shown in Table 4-1.

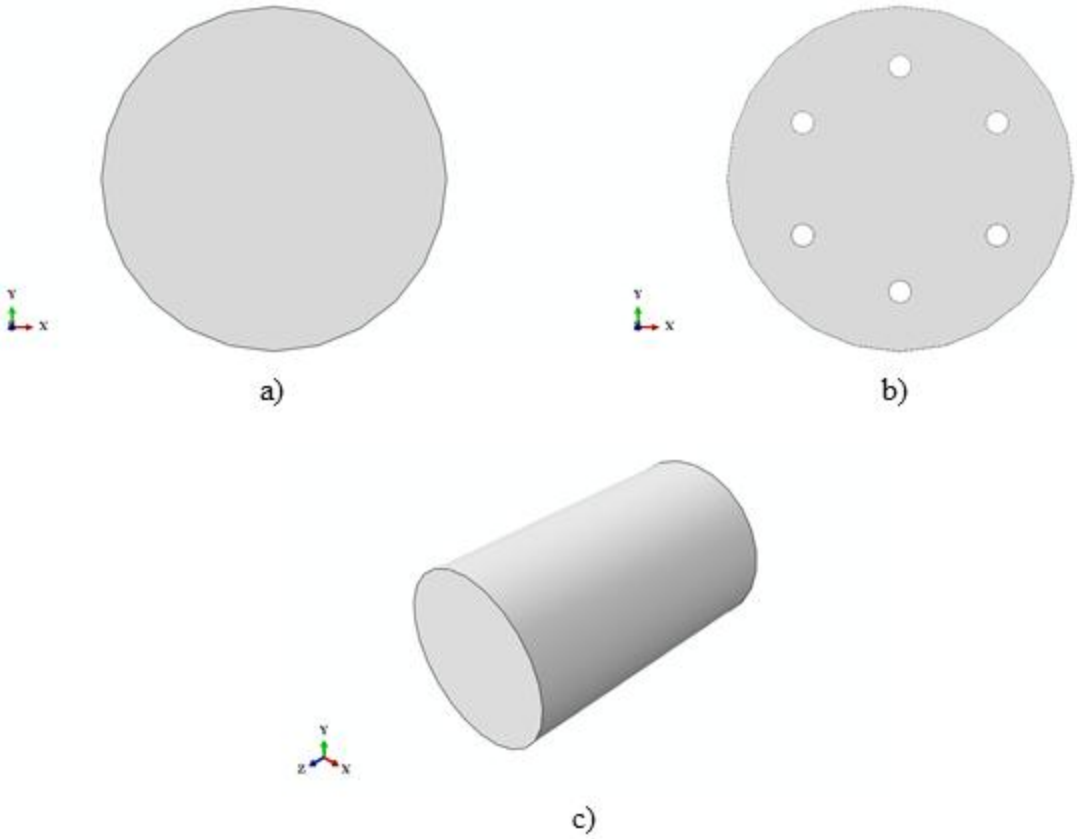

Figure 4-1: Pile model; a) no holes cross section, b) 40 mm holes cross section, c) 3-D view

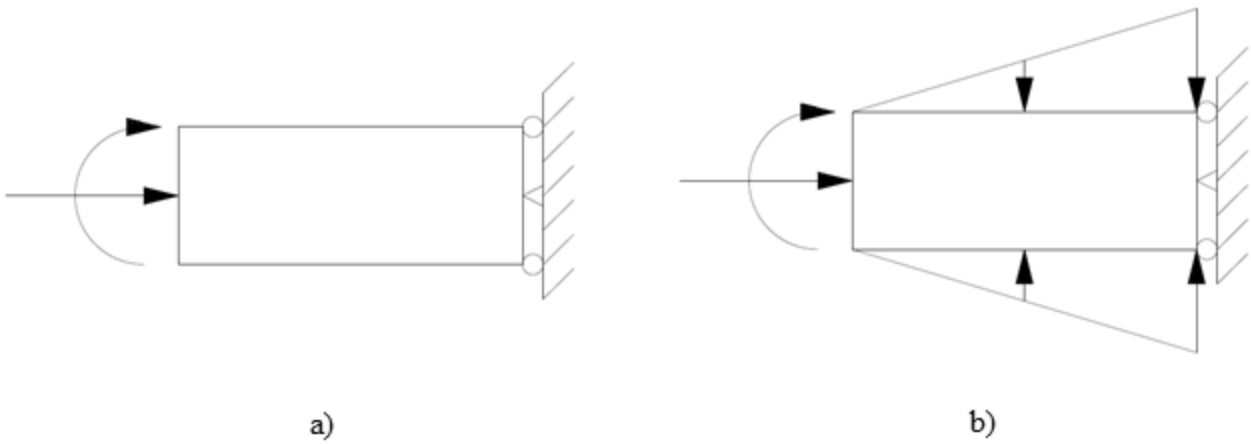

Figure 4-2: General loading and boundary conditions; a) case I, b) case II

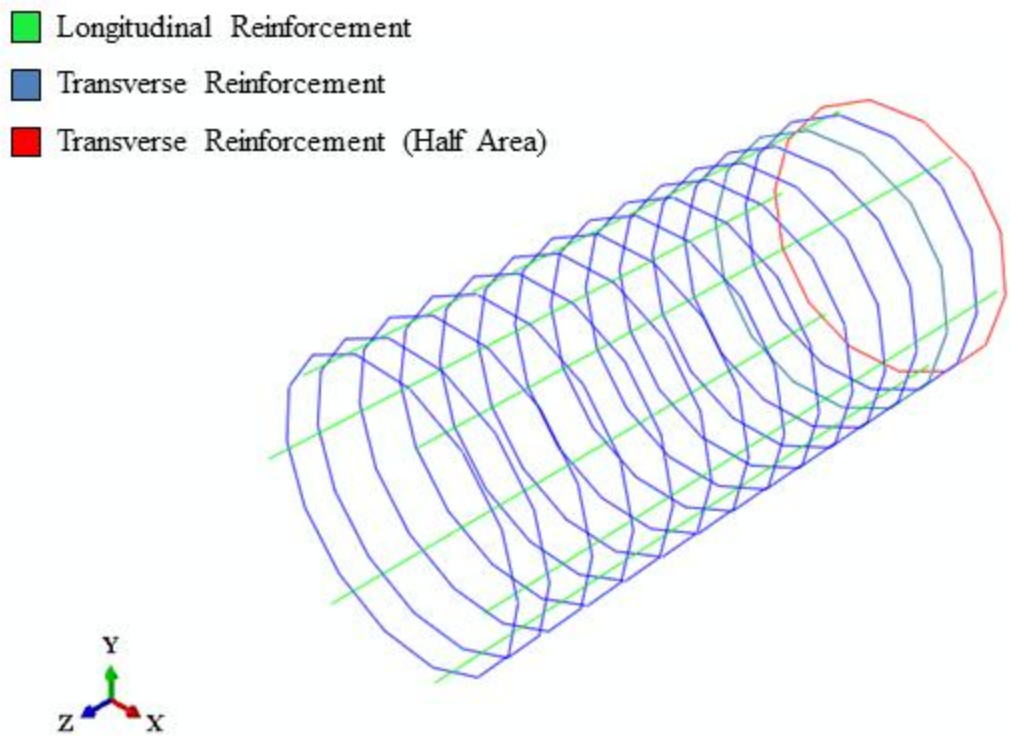

Figure 4-3: Pile reinforcement layout

Table 4-1: Defined steel reinforcement area

Reinforcement Type	Area (m^2)
Longitudinal	7.068E-04
Hoop (Full)	1.539E-04
Hoop (Half)	7.696E-05

Concrete Material Model

Three concrete models are available in Abaqus; a smeared cracking, brittle cracking, and a damage plasticity model to define the inelastic behavior of concrete. The smeared cracking model is designed for monotonic loading at low confining pressures. The brittle cracking model is designed for models governed by tensile strength or cracking failure. The damaged plasticity model is designed for monotonic, cyclic and dynamic loading at low confining pressures. All three concrete models are presented and discussed in detail within the Abaqus User's Manual (Dassault Systèmes SIMULIA, 2012).

The damage plasticity model was chosen because of its ability to characterize cyclic and dynamic loading at low confining pressures. Failure is assumed to be from either compressive crushing or tensile cracking. The damage based plasticity model for concrete was developed using the endochronic theory of plasticity. The yield criterion for the model is based on those by Lubliner et al. (1989) with additional modifications provided by Lee and Fenves (1998). The flow rule is assumed to be nonassociated, yielding a plastic flow rule governed by flow potential (Dassault Systèmes SIMULIA, 2012; Greenwood, 2008).

The tensile and compressive stress strain behaviors of the concrete are shown in Figure 4-4 and 4-5. The behavior for both the tensile and compressive behavior of the concrete is considered linear elastic up to an initial yield stress value. The degradation of the elastic modulus after the initial yield stress is reached is dependent upon a scalar value assigned to both the tensile and compression inelastic strain. However, because the model will consider only monotonic or static loading, the degradation of the elastic modulus will not be prevalent. Damaged material states in tension and compression are handled by independent hardening laws

defined in terms of equivalent plastic strain. Compression hardening is provided in terms of compressive stress as a function of inelastic strain and the inelastic compressive strain rate (Dassault Systèmes SIMULIA, 2012; Greenwood, 2008).

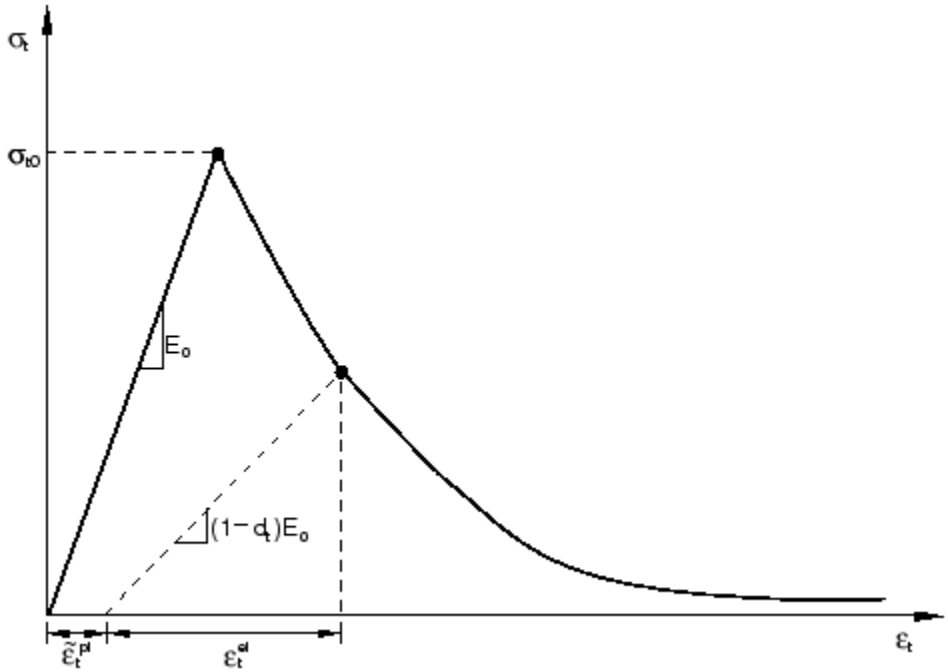

Figure 4-4: Tensile stress strain behavior (Dassault Systèmes SIMULIA, 2012)

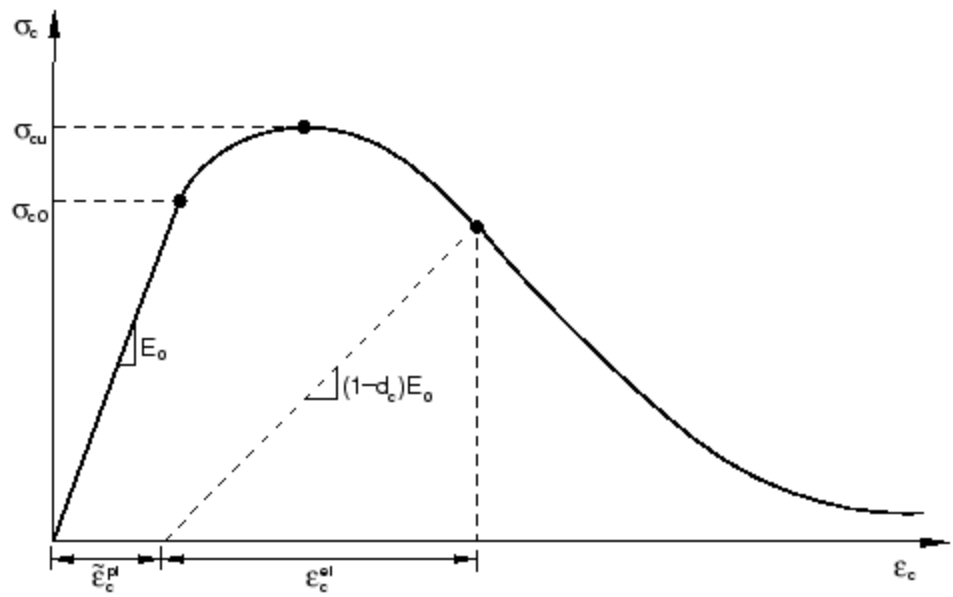

Figure 4-5: Compressive stress strain behavior (Dassault Systèmes SIMULIA, 2012)

Concrete Properties

The elastic behavior of the concrete is assumed to be linear and isotropic. The Young's Modulus and Poisson's Ratio were taken as the default values for a concrete damage-plasticity material verification study and are similar in magnitude to that used in Chapter 3. A summary of these values are shown in Table 4-2.

Table 4-2: Concrete elastic properties

Young's Modulus (MPa)	26475
Poisson's Ratio	0.17

The concrete damaged plasticity model is defined by the following three components: the plasticity behavior, the compressive behavior, and the tensile behavior. The plasticity component of the model is defined by the following five parameters: dilation angle, eccentricity, ratio of initial equibiaxial compressive yield stress to initial uniaxial compressive yield stress, ratio of the second stress invariant on the tensile meridian to that on the compressive meridian, and a viscosity parameter (Dassault Systèmes SIMULIA, 2012; Greenwood, 2008). The dilation angle is measured in the *p-q* plane at high confining pressures. The eccentricity defines the rate at which the flow potential approaches the asymptote. The viscosity parameter defines the relaxation time for the visco-plastic system. The input values for these parameters are summarized in Table 4-3 and were taken from those suggested by the Abaqus User's Manual.

Table 4-3: Concrete plastic behavior parameters

Dilation Angle (°)	15
Eccentricity	0.1
fb0/fc0	1.16
K	0.66
Viscosity Parameter	0.01

The post cracking compressive behavior of the concrete was defined by inputting the yield stress as a function of inelastic strains. Data for these values can be found in Table 4-4 along with the information input for the damage percentage for the inelastic strain values, and they were taken as those used in a material verification study shown in the Abaqus User Manual.

Table 4-4: Concrete compressive behavior

Yield Stress (kPa)	Damage Parameter	Inelastic Strain
24019	0	0
29208	0.1299	0.0004
31709	0.2429	0.0008
32358	0.3412	0.0012
31768	0.4267	0.0016
30379	0.5012	0.002
28507	0.566	0.0024
21907	0.714	0.0036
14897	0.8243	0.005
2953	0.9691	0.01

The tensile behavior of the concrete can be defined using one of three methods: specifying stress as a function of inelastic strain, specifying stress as a function of crack width, or specifying stress as a function of fracture energy. The first approach is used when reinforcement is defined throughout the model, as mesh sensitivity and convergence issues can occur. Mesh refinement and the subsequent decrease in element size can lead to mesh dependent tensile crack bands. This problem is less of a concern if tensile cracking is distributed evenly throughout the model, as would be the case for a substantially reinforced structure. The second and third approach to defining tensile behavior should be used in models that are not substantially reinforced (Dassault Systèmes SIMULIA, 2012; Greenwood, 2008). A reinforcing ratio is not specified by Abaqus for what should be considered heavily reinforced and, therefore, because the model contains both longitudinal and transverse steel, approach one was used. The tensile behavior of the concrete was input by defining yield stresses at varying inelastic strains. The

damage behavior was defined as a damage parameter or damage percentage for the previously input inelastic strains along with the damage parameter can be found in Table 4-5.

Table 4-5: Concrete tensile behavior

Yield Stress (kPa)	Damage Parameter	Cracking Strain
1780	0	0
1457	0.3	0.0001
1113	0.55	0.0003
960	0.7	0.0004
800	0.8	0.0005
536	0.9	0.0008
359	0.92	0.001
161	0.94	0.002
73	0.96	0.003
40	0.98	0.005

The stiffness recovery is important in cyclic loading to define the strength of the concrete when alternating from one stress state to the other. Once concrete reaches a high enough compressive state, crushing can occur. If the loading is alternated to a tensile state, the cracks propagated from crushing result in a loss of strength and no recovery. The opposite is true when going from a tensile state to a compressive state because the crack is closed. Stiffness recovery for both compressive and tensile behavior was input as 1 and 0, respectively.

Steel Properties

Steel was defined using an elastic-plastic material model similar to that used in Xtract. The values used for the Young's Modulus and Poisson's Ratio can be found in Table 3-2, of Chapter 3. The plastic region of the model was defined by yield stress at various inelastic strains. The yield stress after failure was assumed to be minimal rather than zero to limit convergence issues. This value was less than the order of three magnitudes smaller than typical yield stress values at smaller inelastic strains. The input values for the steel plastic material parameters are summarized in Table 4-6.

Table 4-6: Steel plastic material inputs

Yield Stress (MPa)	Inelastic Strain
414	0
414	0.006
483	0.018
552	0.038
620	0.088
1	0.1

Boundary and Initial Conditions

The longitudinal and hoop steel reinforcement was embedded within the concrete pile and a no slip/movement limitation was invoked between the steel and concrete surfaces (Figure 4-6). Loading was applied to the top of the pile head and roller supports at the bottom to reflect

the load distribution in Figure 4-2. The bottom of the pile did not allow for translation in the z direction across. A partition was created through the center of the face which was used to fix translation in the y direction. A point at the center of the face was used to restrict translation in the x direction. These boundary conditions are shown in Figure 4-7.

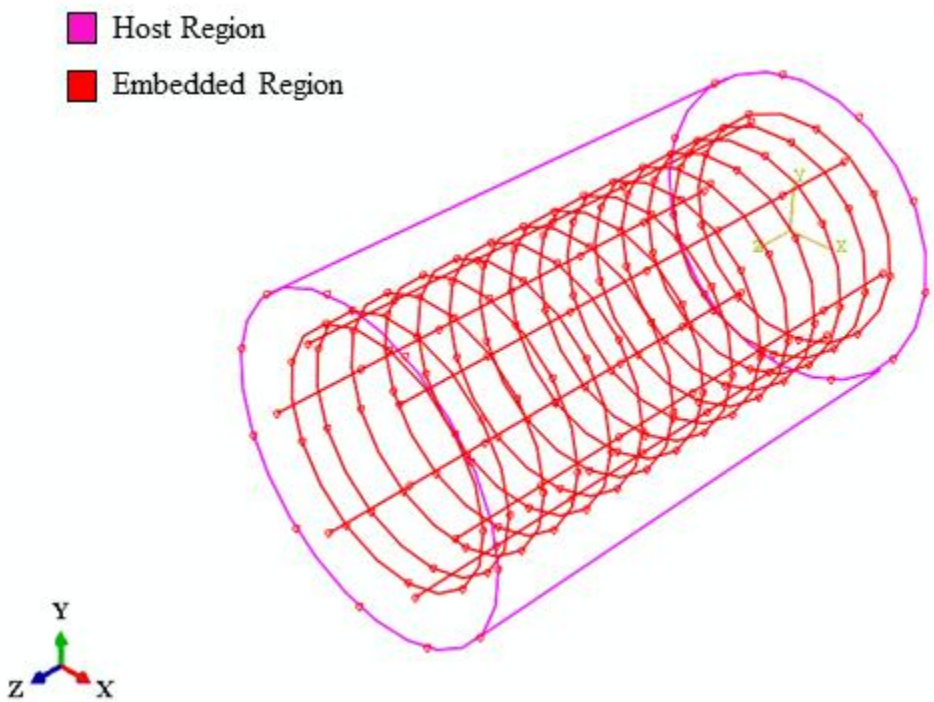

Figure 4-6: Pile contact surface definitions

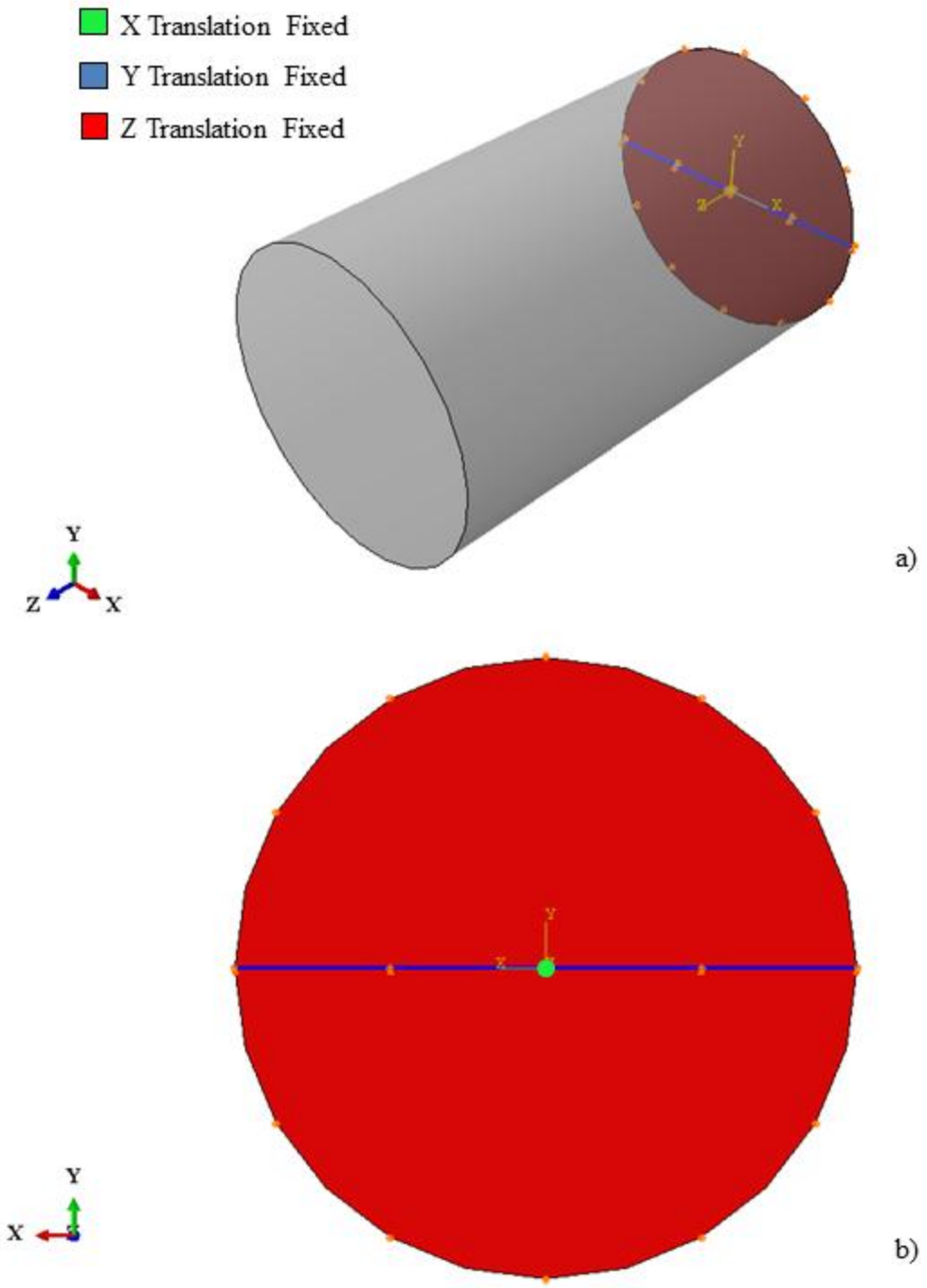

Figure 4-7: Pile boundary conditions

Loading

Two loading cases were analyzed for each pile (Figure 4-2). Loading case I considered only an axial force and moment load applied about the free end of the pile. Loading case II considered an additional confining stress about the circumference of the pile. .

The first step was the application of the axial force. This was achieved by defining surface traction pressure load perpendicular to the free face of the pile (Figure 4-8, a and b). The magnitude of the pressure applied to the two pile types are shown in Table 4-7. Note that the pressure load increases for the cross section with holes because of the decrease in cross sectional are due to the holes. The pressure values are equivalent to a 1MN axial force distributed as a pressure load about the face of each pile type, the same as applied in Xtract.

Table 4-7: Axial pressure loads

Pile Type	Pressure Load (MPa)
40mm Holes	3.634
No Holes	3.537

The second step was the application of the moment. This was achieved by defining a linearly changing pressure with respect to the y-axis on the free face of the pile (Figure 4-8, c and d). The resulting linearly changing pressure load applied a compression load at the top of the free face and reduced in values reaching zero at the middle of the face and an equal size tension force at the opposite side of the face. The magnitude of the linearly changing force was set to be 100 MPa at the edges furthest from the neutral axis, which was a large enough value to ensure

failure of the section. The solution is solved by incrementing the loading and when convergence is not achieved the maximum moment value would be met.

The third step, which only applied to loading case II, was the application of the linear varying pressure about the circumference of the pile (Figure 4-8, e and f). This was applied to simulate the lateral pressure that would be experienced by the pile from the surrounding soil stratum. This was achieved by defining a linearly changing pressure with respect to the z direction and normal to the circumferential surface. The magnitude was specified as 0 kPa at the free end and linearly increased toward the restrained end of the pile. The magnitude of the horizontal stress at the fixed end of the pile was calculated using:

$$\sigma'_h = K_0 \rho g z \tag{4-1}$$

where:

K_0 = coefficient of lateral earth pressure

ρ = density of the soil

g = acceleration due to gravity

z = depth from surface

The density was assumed to be 1800 and 1900 kg/m^3 for sandy and clayey soil, respectively. The coefficient of lateral earth pressure for sandy soil was determined using (Jaky, 1948):

$$K_0 = 1 - sin\phi' \tag{4-2}$$

where:

ϕ' = internal friction angle

Two confinement pressures were analyzed for sandy soil by assuming an internal friction angle of 30° and 45°. The resulting coefficient of lateral earth pressures were 0.5 and 0.29, and stress magnitudes of 8.83 and 5.17 kPa at the restrained end of the pile, for the 30° and 45° internal friction angle, respectively.

The coefficient of lateral earth pressure for clayey soil was determined using (Mayne and Kulhawy, 1982):

$$K_0 = (1 - sin\phi')OCR^{sin\phi'} \tag{4-3}$$

where:

OCR = over consolidation ratio

Two confinement pressures were also analyzed for clayey soil. An internal friction angle was assumed to be 30° and an over consolidation ratio of 1 and 8 yielded coefficient of lateral earth pressure values of 0.5 and 1.41, and stress magnitudes of 9.32 and 26.35 kPa at the restrained end of the pile, respectively. A summary of the assumptions for each soil type and confinement pressure are included in Table 4.8.

Table 4-8: Confinement loading summary

Soil Type	ϕ’	K_0	Max Pressure (kPa)
Clay	30°	0.5	9.32
Clay	30°	1.41	26.35
Sand	30°	0.5	8.83
Sand	45°	0.29	5.17

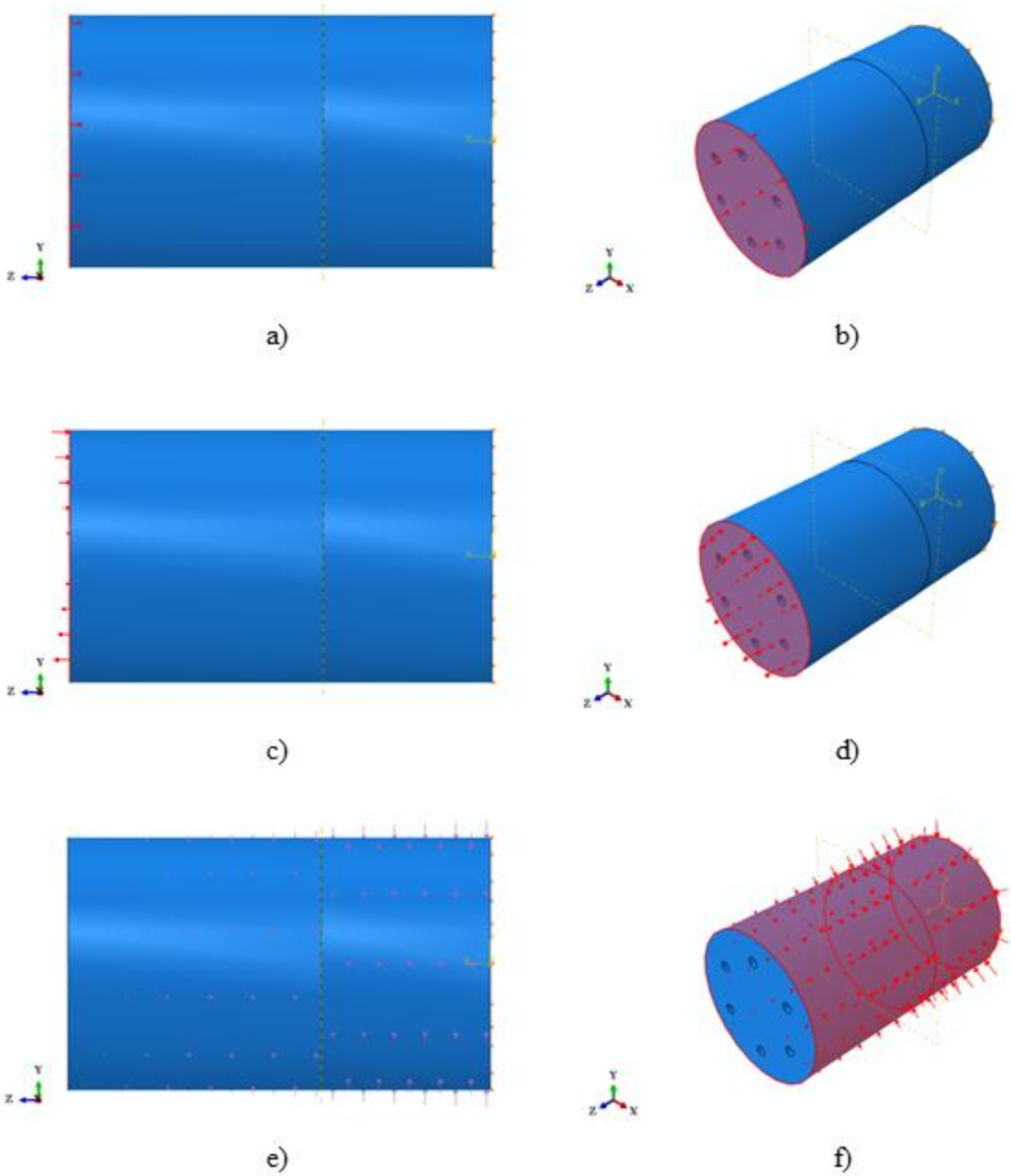

Figure 4-8: Loading conditions; a and b) axial force, c and d) moment, e and f) confining pressure

Elements and Mesh

The elements chosen for the elastic and damage based concrete was an 8-node linear brick with reduced integration and hourglass control (C3D8R). The 8-node reduced integration element was chosen because at refined meshes the computation time will be less than that for larger amount of nodes at full integration. The elements chosen for the longitudinal and hoop steel was a 2-node linear 3-D truss (T3D2). The global continuum element mesh sizes included 0.1, 0.05, and 0.03 m. The sizes included a coarse mesh, 0.1 m, to a very fine mesh, 0.03 m. The global element size for truss elements was set at 0.1 m for all meshes. The complete mesh for each of the three global mesh sizes are shown in Figure 4-9.

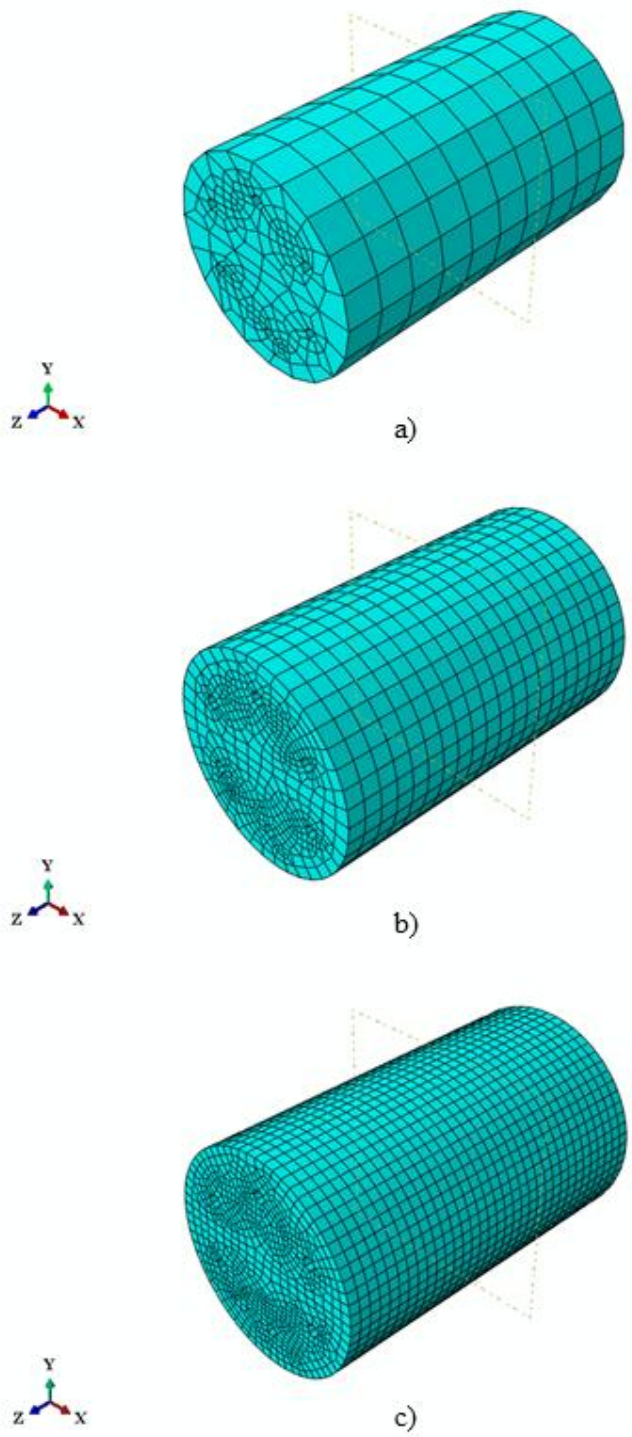

Figure 4-9: Continuum element mesh sizes; a) 0.1 m, b) 0.5 m, c) 0.03 m

Results

The results from the loading case 1 showed that the tensile cracking behavior caused convergence issues which left the model cutting out at lower moment-curvature values than predicted by Xtract. Maximum step times reached for the piles and various global mesh sizes are included in Table 4-9. The larger the maximum time increment reached the larger the moment value that was reached from the specific model.

Table 4-9: Summary of analysis results for pile and mesh types

Pile Types	Maximum Time Increment (sec)	Time for Simulation (sec)	Global Mesh Size (m)
No Holes	1.817	146	0.1 for continuum and 0.1 for truss elements
40 mm Holes	1.600	261	
No Holes	1.485	443	0.05 for continuum and 0.1 for truss elements
40 mm Holes	1.217	293	
No Holes	1.549	9130	0.03 for continuum and 0.1 for truss elements
40 mm Holes	1.436	14244	

The results of the moment-curvature for the finite element cross section and with mesh size are shown in Figure 4-10. The moment was calculated by averaging the moment computed by Abaqus at the boundary between the support and the elastic and plastic interface. The curvature was computed by finding the change in angle at the elastic and plastic concrete interface and dividing by the length from the support. At very low curvature values two distinct slopes are observed from the Xtract results. The difference in slope is due to the initial tensile cracking of the concrete. This is observed in the finite element model as well for all cross section and mesh sizes. As the mesh is refined the moment at which this cracking occurs and the slope of

both the initial and post cracking moment-curvature diagram approaches that predicted by Xtract. There is also no substantial observed difference between cross sections of the refined mesh as they both change slope at about 0.17 MN-m.

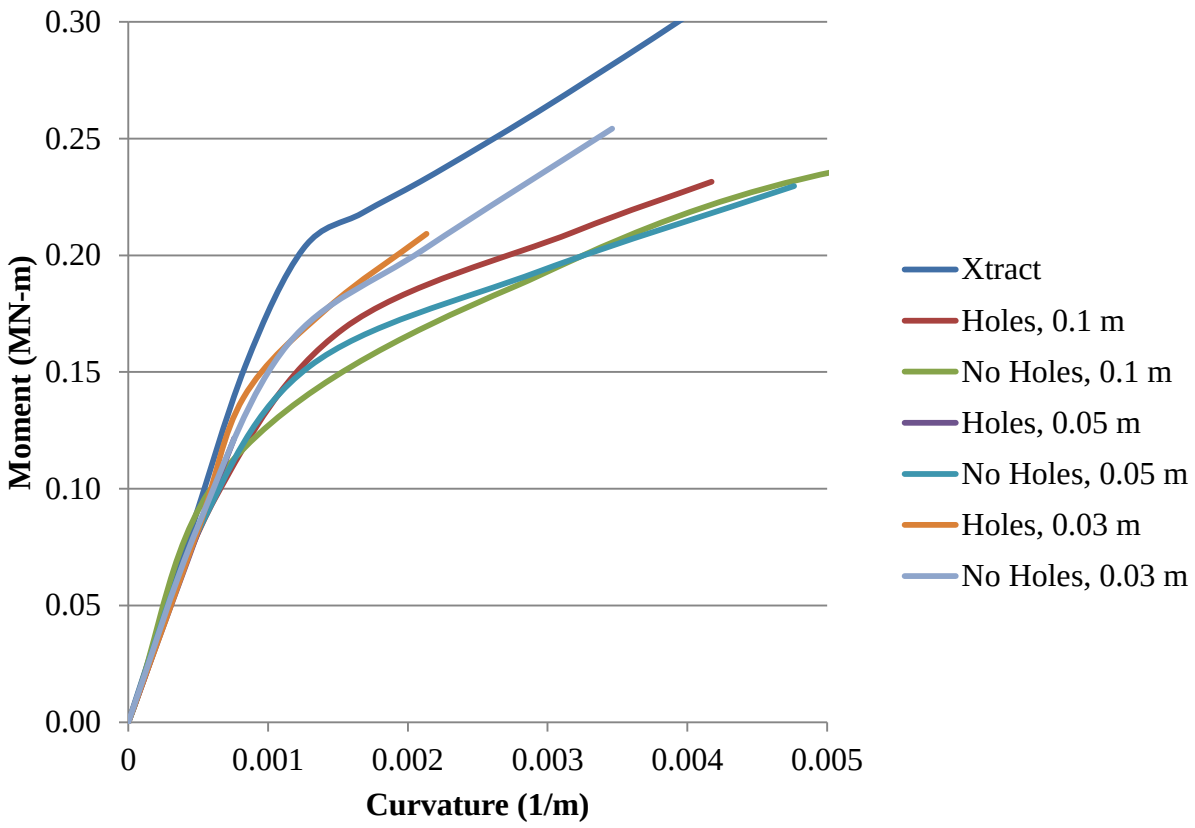

Figure 4-10: Abaqus moment-curvature predictions with mesh size

The tensile cracking damage of both the model with and without holes produced similar results. Severe tensile cracking occurred at both the boundary between the elastic and damage plasticity concrete material as well as one element layer removed from the boundary conditions (Figure 4-11). The cracking was shown to occur up to and above the middle of the pile, similarly as seen with the Xtract model.

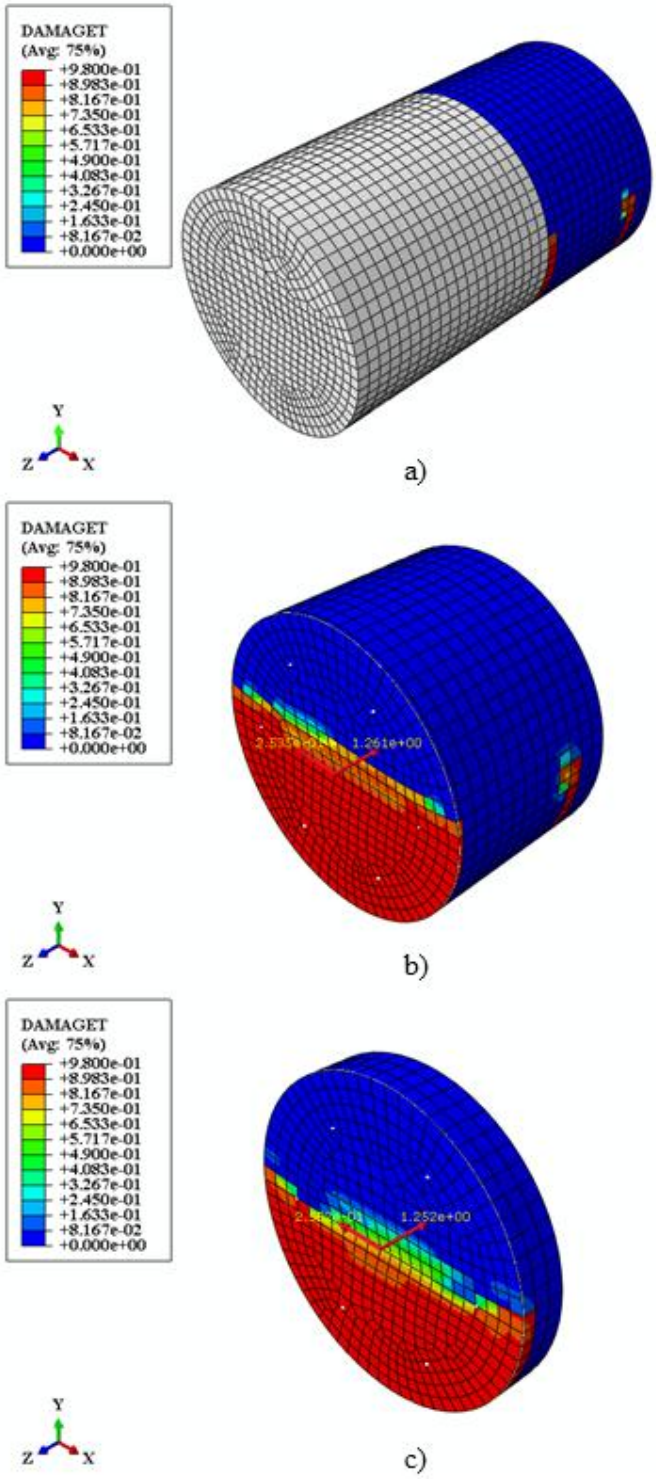

Figure 4-11: Tensile damage; a) whole pile, b) elastic/plastic boundary, c) near support

The results from loading case II, with additional confinement pressure, did not greatly alter the results of the model. This may be due to the material model of the concrete damage model, which does not consider changes due to confinement pressures and, because of that, is designed for uses at very low confining pressures. Compared to the compressive and tensile behavior of the concrete, the confinement pressure is on the order of a few magnitudes lower than that of the maximum tensile behavior which may also be a reason for the lack of change in the results.

The preliminary results showed that the pile sustained serious cracking due to tensile stresses and strains, but that the pile was not able to reach past between 40 to 60 percent of the maximum moment predicted by Xtract. Abaqus was unable to converge at higher stresses and hence higher moments because of the substantial tensile cracking. Different techniques, such as stabilization during loading steps, changes of concrete tensile behavior input, and alteration of solution method, were used to advance the analysis further but were not successful.

CHAPTER 5

CONCLUSIONS AND RECOMMENDATIONS

Summary

The effect of the removal of concrete from the placement of vertical heat absorber tubing on the structural performance of geothermal reinforced concrete piles under axial and moment loading was analyzed using the programs Xtract and Abaqus. The focus of the analysis was on the effect of heat exchanger tubing diameter and placement, transverse and longitudinal reinforcement size and placement, as well as soil type on structural performance.

Five cross sections were analyzed using Xtract, each with a pile diameter of 600 mm, having varying changes to the cross section due to being with and without heat absorber tubing (Figure 3-2). Material models were designed and specified for the confined concrete, unconfined concrete, and longitudinal steel. A comparison of the cross sections showed very little difference in the moment-curvature response about both axes, except for the cross section that considered holes with all concrete to be unconfined (Figure 3-3 and 3-4). Cross sections that included 40 mm tubing holes evenly spaced between the longitudinal steel, as well as varying degrees of unconfined concrete surrounding the holes performed nearly identical up to curvature values of 0.02 1/m. At larger curvature values, 0.1 1/m, the moment of the geothermal reinforced concrete piles decreased by between 1 and 7 percent, compared with the conventional reinforced concrete pile (Table 3-3 and 3-4). Differences between the conventional reinforced concrete and the cross section with defined 40 mm holes and all unconfined concrete was much greater, between 50 and

60 percent. Marginal differences between the moment-curvature response about the x and y axes are due to the movement of the neutral axis and alignment with longitudinal steel bar pairs (Figure 3-5).

A three dimensional pile model with two cross sections was analyzed using the finite element program Abaqus. The pile cross sections included a 600 mm diameter case with no holes and a case with 40 mm holes evenly spaced between the longitudinal reinforcement (Figure 4-1). The pile length was 1 m, and 0.6 m of the length was modeling as elastic concrete near the loading end, and the remaining length of model was assumed to be a concrete damage model. The embedded longitudinal and hoop reinforcement followed an elasto-plastic model. The pile was restrained about one end (Figure 4-7), and loaded (Figure 4-8). Convergence issues from tensile crack propagation prevented the model from reaching the maximum moment value predicted by Xtract at curvature values around 0.02 1/m. Instead, a value of between 20 to 60 percent of the maximum moment values predicted by Xtract was reached before convergence issues caused the analysis to terminate. Tensile cracks formed in two locations, near the support or boundary conditions, and at the boundary between the elastic and damage concrete materials (Figure 4-11). The curvatures of the refined mesh were about 30 percent lower than that predicted by Xtract. The strain was nearly linear throughout the cross section of the pile from the applied moment loading, similar to that of Xtract.

Conclusions

From the results of both the Xtract and Abaqus models the following conclusions are drawn:

- The structural performance of geothermal reinforced concrete piles is nearly identical to that of conventional reinforced concrete piles under static loading (axial and moment).
- Xtract provides adequate and accurate results of reinforced concrete piles up to small curvatures.
- Two dimensional analysis (Xtract) can further predict and provide results that three dimensional analysis (Abaqus) cannot, due to limitations of elements and the solver of the software.
- The structural performance of the pile is heavily dictated by the longitudinal reinforcement rather than the confined and unconfined concrete of the pile.
- The transverse reinforcement dictates changes to the confined (core) concrete of the pile which only marginally affects the structural performance.
- The size and spacing of heat absorber tubing and the subsequent removal of concrete only marginally affects the structural performance at very high curvatures.

Recommendations for Further Research

The following recommendations are proposed for further research in this area:

- Development of methods to quantify the effect the heat absorber tubing and subsequent removal of concrete on the confined concrete strength in the core of piles.
- Dynamic analysis of conventional and geothermal reinforced concrete piles using finite element models.

- Additional field studies to compare and refine prediction models for geothermal piles.
- Measurement of end conditions, such as pile restraint to provide additional information for prediction models.

REFERENCES

Abaqus Software and Documentation, Version 6.11-1. © Dassault Systèmes, SIMULIA, 2012.

ACI Committee, American Concrete Institute, & International Organization for Standardization. (2008). Building Code Requirements for Structural Concrete (ACI 318-08) and Commentary. American Concrete Institute.

Amatya, B. L., Soga, K., Bourne-Webb, P. J., Amis, T., & Laloui, L. (2012). Thermo-mechanical behaviour of energy piles. *Geotechnique*, 62(6), 503-519.

Balendra, S. (2005). Numerical Modeling of Dynamic Soil-Pile-Structure Interaction. *Washington State University*. Pullman, Washington

Bourne-Webb, P. J., Amatya, B., Soga, K., Amis, T., Davidson, C., & Payne, P. (2009). Energy pile test at Lambeth College, London: geotechnical and thermodynamic aspects of pile response to heat cycles. *Géotechnique*, *59*(3), 237-248.

Bourne-Webb, P. J., Amatya, B., & Soga, K. (2012). A framework for understanding energy pile behaviour. *Proceedings of the ICE-Geotechnical Engineering*, *166*(2), 170-177.

Brandl, H. (2006). Energy foundations and other thermo-active ground structures. *Geotechnique*, 56(2), 81-122.

Coduto, Donald P. Foundation Design: Principles and Practices. 2nd ed. *Prentice Hall, 2001*, Upper Saddle River, NJ:. Print.

Greenwood, S. M. (2008). Analytical Performance Evaluation of Hollow Prestressed Piles and Pile-Cap Connections in the I-5 Ravenna Bridge. *Washington State University*. Pullman, Washington

Jaky, J. (1948). Pressure in silos. Proc., *2nd Int. Conf. on Soil Mechanics and Foundation Engineering*, Rotterdam, The Netherland, 1, 103–107.

Johnston, I. W., Narsilio, G. A., & Colls, S. (2011). Emerging geothermal energy technologies. *KSCE Journal of Civil Engineering*, *15*(4), 643-653.

Knellwolf, C., Peron, H., & Laloui, L. (2011). Geotechnical Analysis of Heat Exchanger Piles. *Journal of Geotechnical and Geoenvironmental Engineering*, 137(10), 890-902.

Laloui, L., Nuth, M., & Vulliet, L. (2006). Experimental and numerical investigations of the behaviour of a heat exchanger pile. *International Journal for Numerical and Analytical Methods in Geomechanics*, 30(8), 763-781.

Laloui, L., & Di Donna, A. (2011). Understanding the thermo-mechanical behaviour of energy piles. *Civil Engineering*, *164*, 184-191.

Lee, J., & Fenves, G. L. (1998). Plastic-damage model for cyclic loading of concrete structures. *Journal of engineering mechanics*, *124*(8), 892-900.

Liu, G. R., & Quek, S. S. (2003). The finite element method: a practical course. *Butterworth-Heinemann*, Boston

Lubliner, J., Oliver, J., Oller, S., & Oñate, E. (1989). A plastic-damage model for concrete. *International Journal of Solids and Structures*, *25*(3), 299-326.

Mander, J. B., Priestley, M. J., & Park, R. (1988). Theoretical stress-strain model for confined concrete. *Journal of structural engineering*, *114*(8), 1804-1826.

Mayne, P. W., and Kulhawy, F. H. (1982). K_0 – OCR relationship in soil. *J. Geotech. Eng. Div., Am. Soc. Civ. Eng.*, 1086, 851–872.

Olgun, C. G., Abdelaziz, S. L., & Martin, J. R. (2013). Long-Term Performance and Sustainable Operation of Energy Piles. *Developing the Frontier of Sustainable Design, Engineering, and Construction* (pp. 534-542). ASCE.

Ouyang, Y., Soga, K., & Leung, Y. (2011). Numerical Back-Analysis of Energy Pile Test at Lambeth College, London. *Paper presented at the Proc. ASCE GeoFrontiers 2011 Conf.*, Dallas, TX, Han, J. and Alzamora, DE, eds.

Xtract Software and Documentation, Version 3.0.10. TRC/Imbsen Software Systems, Inc., 2001.